NTNU – Trondheim
Norwegian University of
Science and Technology

The Potential of Hydrophilic Silica Nanoparticles for EOR Purposes

A literateur review and an experimental study

Bjørnar Engeset

Earth Sciences and Petroleum Engineering
Submission date: May 2012
Supervisor: Ole Torsæter, IPT

Norwegian University of Science and Technology
Department of Petroleum Engineering and Applied Geophysics

Abstract

As the world's population is expanding, the global demand for energy will continue to increase. The global demand for all energy will grow by over 50 % the next 25 years(1). New technology and renewable energy will help us face these challenges, but an essential breakthrough in oil and gas production and exploration is also needed. The most common method for secondary oil recovery is water flooding implemented early during the primary production phase. This is done by forcing water down the injection wells in order to maintain reservoir pressure above bubble point, and to sweep the oil towards the production wells.

Micro- and nano- technologies have already proved to be important in technical advances in a variety of industries, and the potential in upstream petroleum industry is great. Nanotechnology will have the ability to improve the industry when it comes to energy supply, by introducing technologies that are more efficient, and more environmental friendly. Many materials, tools and devices with qualities that cannot be matched by conventional technologies can be developed using nanotechnology(2).

In this master's thesis I will look at the unique possibilities of using nanotechnology in oil and gas E&P. The thesis expands my project thesis, where I studied the potential for nanotechnology in exploration, drilling, production and especially enhanced oil recovery. Some believe that nanotechnology has the opportunity to increase the recovery factor up to 10 % in the future(3). This can be achieved by using for example tailored surfactant that can be added to the reservoir in a more controlled way than existing substances. Other applications could be smart fluids and new metering techniques for use in upstream petroleum industry(4).

Experimental studies of the potential of hydrophilic silica nanoparticles have been carried out. Core flood experiments using Berea sandstone were performed to assess the potential in nanoparticle flooding. Permeability impairment was studied by flooding,

and clear identification of retention was observed. It showed that concentration, injection volume and rate are important parameters when injecting particles through a porous media. Scanning Electron Microscope (SEM) was applied to detect any residual particles inside the core sample, which could explain permeability impairments. Further, implementations of silica nanofluid as both secondary and tertiary recovery method were tested. The results showed little mobilization when implemented as tertiary recovery method, but a clear reduction of residual oil saturation was observed when applying as secondary recovery method. Using nanoparticles in EOR is currently only tested at laboratory scale, but integrating this in large scale fields could improve the lifetime, recovery and make oil production even more economically beneficial. This thesis summarizes available information within the topic, and performs laboratory experiments in order to study the potential of hydrophilic silica nanoparticles for EOR purposes.

Sammendrag

Det globale behovet for energi vil fortsette å øke de kommende årene. Ny teknologi og fornybar energi vil hjelpe oss å møte disse utfordringene, men et gjennombrudd i olje- og gassproduksjon er nødvendig. Mikro og nanoteknologi har allerede vist seg å være viktig for tekniske fremskritt i en rekke bransjer, og potensialet i oppstrøms petroleumsvirksomhet er stort. Utvikling av materialer, verktøy og utstyr med kvaliteter som ikke kan oppnås gjennom konvensjonell teknologi, kan oppnås ved hjelp av nanoteknologi(2).

I denne masteroppgaven har jeg sett på de unike mulighetene for nanoteknologi i olje og gass E&P. Avhandlingen bygger videre på prosjektoppgaven, hvor potensialet for nanoteknologi innen leting, boring, produksjon og spesielt innen økt oljeutvinning ble studert.

Eksperimentelle studier av potensialet til hydrofile silisium nanopartikler ble gjennomført. Fløming av Berea sandstein ble utført, og reduksjon i permeabilitet som følge av denne fløm,ingen ble studert. Klare indikasjoner på retensjon ble observert, og konsentrasjon, injeksjonsvolum og rate viste seg å være viktige parametere ved fløming av nanopartikler. Videre ble Scanning Electrom Microscope (SEM) brukt til å påvise retensjon av partikler inne i kjerneprøvene. I tillegg til utførelse av eksperimenter hvor silisium nanopartikler ble anvendt for økt utvinning av olje. Resultatene viste liten mobilisering av olje når partiklene ble anvendt som tertiær utvinningsmetode, mens en tydelig reduksjon i residuell oljemetning ble observert ved sekundær fløming. Nanopartikler er foreløpig bare testet på laboratorienivå, men anvendelse i virkelige olje- og gassfelt kan øke levetiden, utvinningsgraden, samt være økonomisk gunstig i fremtiden.

Acknowledgements

This master's thesis was carried out at the Norwegian University of Science and Technology, Department of Petroleum Engineering and Applied Geophysics during the spring of 2012. I would like to thank my supervisor, Ole Torsæter, for guidance and discussions throughout the process. I will also address a great thank to Roger Overå for his assistance and availability in the laboratory.

All laboratory work was performed together with Ph.D. student Luky Hendraningrat. Planning, execution and discussion of laboratory experiments was done in cooperation with Luky and supervisor Ole Torsæter. I would therefore address a great thank to Luky Hendraningrat for help, guidance and excellent collaboration throughout the whole semester. Ph.D. student, and friend of Luky, Suwarno was of great help concerning the use of SEM-apparatus at the Department of Materials Science and Engineering.

The work in this thesis was made independently and in accordance with the rules set down by the Examination Regulations made by the Norwegian University of Science and Technology.

Bjørnar Engeset

Trondheim 10.06.2012

Contents

List of Figures

LIST OF FIGURES

LIST OF FIGURES

List of Tables

LIST OF TABLES

1

Introduction to Nanotechnology

Nanometer technology originated at the end of the 1980's and has developed into a new high technology, by which new materials can be formed by rearranging atoms or molecules(5). It is believed that nanotechnology will introduce many cutting-edge applications in the coming years. In this chapter, the most important properties of nanoparticles (NP) are mentioned. A wider study of nanoparticle properties, and a study of present and further nanotechnology applications was done in the project thesis, and is therefore not mentioned here(6).

1.1 What is Nanotechnology?

A nanometer is one thousand millionth of a meter. In comparison, a red blood cell is approximately 7,000 nm wide and a water molecule is almost 0.3 nm across(7). There are different definitions of the range of the nanoscale, but it is usually defined to be from 100 nm down to approximately 1 nm. Nanotechnology is the term that is used to cover design, construction and utilization of functional structures with at least one characteristic dimension measured in nanometer(8). What distinguishes nanotechnology and nano-structure from other technologies is the special properties that are unique in terms of its nanoscale proportions. Composites made from particles of nano-size metals smaller than 100 nm can become stronger than anticipated by existing material-science models. This drastic change in properties may be due to two reasons. Nanomaterials have a relatively high surface area when compared to the same mass of materials produced in larger scale, which can enhance strength, electrical

properties and make materials more chemical reactive. In addition, quantum effects can be dominating, affecting the optical, electrical and magnetic behavior of materials(7). These nanostructured materials and systems are classified with respect to the number of dimensions which lie within the nanometer range, confined in either one, two or three dimension system(8).

1.2 Properties

Atoms, molecules and solids are the basic building blocks of nanotechnology. Material properties are determined by the cooperative effect of a huge number of similar particles in a three-dimensional arrangement(9). When it comes to solid materials, the properties of a surface may differ from the bulk conditions, where the number of surface atoms is small compared to the number of bulk particles. In the case of nanotechnology, this ratio is inverted. This relates the properties of nanostructure more closely to the state of individual molecules, or molecules on the surface or interface, rather then properties of the bulk material(9).

1.2.1 Structural Properties

Nanoparticles have a high surface area to volume ratio. Decreasing particle size in addition with increasing surface area leads to changes in interatomic spacing. This effect can be related to the compressive strains induced by internal pressure as a consequence to the small radius of curvature in the nanoparticles. There is also an apparent stability of metastable structures in small nanoparticles and clusters. Small nanoparticles and nano-dimensional layers may adopt a different crystal structure than normal bulk material (8).

1.2.2 Chemical Properties

Reduction of system size may change the chemical reactivity because of the increase in surface area to volume ratio. Catalysis using finely divided nanoscale systems can increase the rate, selectivity and efficiency of chemical reactions such as combustion or synthesis, whilst simultaneously significant reducing waste and pollution. It is also observed that nanoparticles change chemical behavior distinct from larger counterparts.

A substance may for example not be soluble in water at micro scale, but will dissolve easily when at nanostructure scale(8).

1.2.3 Mechanical Properties

Mechanical properties are dependent on the ease of the formation or the presence of defects within a material. When the system size decreases, the ability to support such defects become more difficult, and mechanical properties will be altered correspondingly(8). Single-walled carbon nanotubes have proved to be stronger than steel due to its high mechanical strengths(7). In addition, many nanostructured metals and ceramics are observed to be super elastic. They have the ability to undergo extensive deformation without necking or fracture(8). These are properties that extend the current strength-ductility of conventional materials, and give nanomaterials a great advantage when it comes to mechanical properties.

1.3 Production Methods

There are several ways to fabricate nanostructures. Richard Faynman had the original vision, to arrange the atoms the way we wanted, which ended up as the "bottom-up" approach. This approach fabricated methods at the atomic or molecular scale, using self-organization and self-assembly of the individual building blocks(10). On the other hand, the "top-down" approach is much simpler and relies on miniaturization of bulk fabrications(8).

1.3.1 "Bottom-up" Process

The "bottom-up" method includes chemical synthesis and/or highly controlled deposition and growth of materials. The chemical synthesis may be carried out in either vapor, liquid or solid phase. Obtaining nanoscale systems via the solid state is difficult, and vapor and liquid fabrications are therefore most common(8). The "bottom-up" nanofabrication is based on building nanostructures atom by atom using either self-assembly techniques or manipulation of atoms by employing scanning probing microscopy(11).

1.3.2 "Top-down" Process

The "top-down" method is simpler and relies either on the removal or division of bulk material, or to produce the desired structure with suitable properties by miniaturizing bulk fabrication process(8). The approach is based on physical and micro-lithographic philosophy, which is a contrast to the "bottom up"-method, where atomic or molecular units are used to assemble molecular structures(9). There are several ways of fabrication regarding the "top-down" approach. Milling, which is known as mechanical attrition or mechanical alloying, is a technique that can be operated in a large scale, hence making it interesting for the industry. The most common method is the lithographic process. This process uses either X-rays, ultraviolet light, electrons or ions to project an image containing a given pattern onto a photo-resisting surface(8). One of the advantages regarding the "top-down" approach is that the parts are both patterned and built in place, so no assembly step is required(11).

2

Reservoir and Fluid Properties

Knowledge of rock and fluid properties are of essential importance to understand the behavior and principles of a reservoir. Rock and fluid properties are usually determined by laboratory experiments on core samples of actual reservoir fluids. This chapter will address the most important reservoir and fluid properties.

2.1 Reservoir Properties

2.1.1 Porosity

Beside permeability, porosity is considered the most important reservoir property. Porosity is the measurement of storage capacity of a reservoir. It is defined as:

$$\phi = \frac{porevolume}{bulkvolume} = \frac{bulkvolume - grainvolume}{bulkvolume} \tag{2.1}$$

There are two different types of porosity. Absolute, or total porosity, is the ratio of all pore spaces in the rock to the bulk volume of the rock, while effective porosity is the ratio of interconnected void spaces to bulk volume. Of these two, only the effective porosity contains fluids that can be produced. For highly cemented rocks like eq. shale, the difference between total and effective porosity may be significant. While for granular materials like sandstone the effective porosity approaches the total porosity.

During deposition of sediments, primary porosity is developed. After deposition, due to geological processes subsequent to formation of the deposit, secondary porosity is formed. These changes in the origional pore space can be created by eq. ground stresses or water movement(12).

2.1.2 Permeability

Permeability is the ability or measurement of a rocks ability to transmit fluids. Formations that transmit fluids readily are described as permeable and tend to have many large, well-connected pores. Shales and siltsotens are defined as impermeable formations, with finer or mixed grain size, and with smaller, fewer, or less interconnected pores(13). Permeability may be expressed through Darcy's equation:

$$\frac{q}{A} = \frac{k}{\mu}\frac{dP}{dx} \tag{2.2}$$

Permeability, or absolute permeability, is referred to as 100 % saturation of a single face, while effective permeability is the ability of the porous material to conduct a fluid when its saturation is less than 100 % of the pore space(12).

2.1.3 Relative Permeability

Relative permeability is the ratio of the effective permeability of a given phase, eq. oil in presence of other phases, to the absolute permeability:

$$k_{ro} = \frac{k_o}{k} \tag{2.3}$$

The relative permeability is influenced by several factors like wettability, saturation, temperature, pore geometry and viscous, capillary and gravitational forces. Oil and water relative permeabilities are usually plotted as a function of water saturation. As seen in Figure 2.1, there are two different curves, drainage and imbibitions. Drainage

is when the wetting phase is decreasing, while imbibition is when the wetting phase is increasing in magnitude. These two recovery mechanisms, drainage and imbibiton, are discussed in the project thesis and therefore not further explained here(6). The curves consist of three important elements; the end point fluid saturations, end point permeabilities and the curvature of the relative permeability function. Especially the end point saturations are of interest as they are directly related to the recoverable oil. The end point relative permeabilities are used in the mobility ratio calculations and tell us about the sweep efficiency of a displacement process(12).

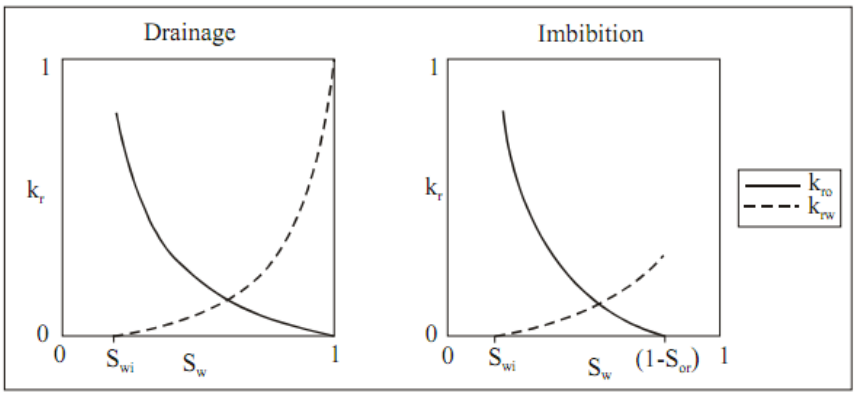

Figure 2.1: Relative Permeability - Drainage and imbibition curves for oil and water(12).

The concept of relative permeability is fundamental to the study of simultaneous flow of immiscible fluids thorugh porous media. For oil and water, we have the following equations:

$$q_w = \frac{k_w A}{\mu_w}(\frac{dP}{dx} + \rho_w g sin\alpha) \tag{2.4}$$

$$q_o = \frac{k_o A}{\mu_o}(\frac{dP}{dx} + \rho_o g sin\alpha) \tag{2.5}$$

By defining these two equations, the fractional flow equation for the displacement of oil by water can be obtained.

2.1.4 Wettability

Wettability of a reservoir rock-fluid system is defined as the ability of one fluid in the presence of another to spread onto the surface of the rock. Wettability plays an important role in the production of oil and gas because it is a main factor in the flow processes in the reservoir rock, as well as determine initial fluid distribution(12). Rocks may be water-wet, oil-wet or intermediate-wet. The intermediate state between oil-wet and water-wet can be caused by a mixed-wet system where some surfaces are oil-wet and other water-wet, or a neutral system where surfaces are not strongly wet by neither water nor oil(14). Wettability of a rock will depend on many factors like rock material and pore geometry, geological mechanisms, composition and amount of oil and brine, pressure and temperature, and mechanisms occurring during production(12).

2.1.5 Capillary Pressure

When a discontinuity in pressure between two immiscible fluids exists across the interface separating them, this difference in pressure is called capillary pressure. The capillary pressure is defined as the difference between the pressure in the non-wetting phase and the pressure in the wetting-phase.

$$P_c = P_{non-wetting} - P_{wetting} \tag{2.6}$$

The capillary pressure can have both positive and negative value, and the conditions for capillary forces to exist are a certain curvature of the fluid-fluid interface. The relationship between saturation and capillary pressure is a function of wettability, pore sizes, interfacial tension and fluid saturation history. In Figure 2.2 the relationship between capillary pressure and water saturation can be seen(12).

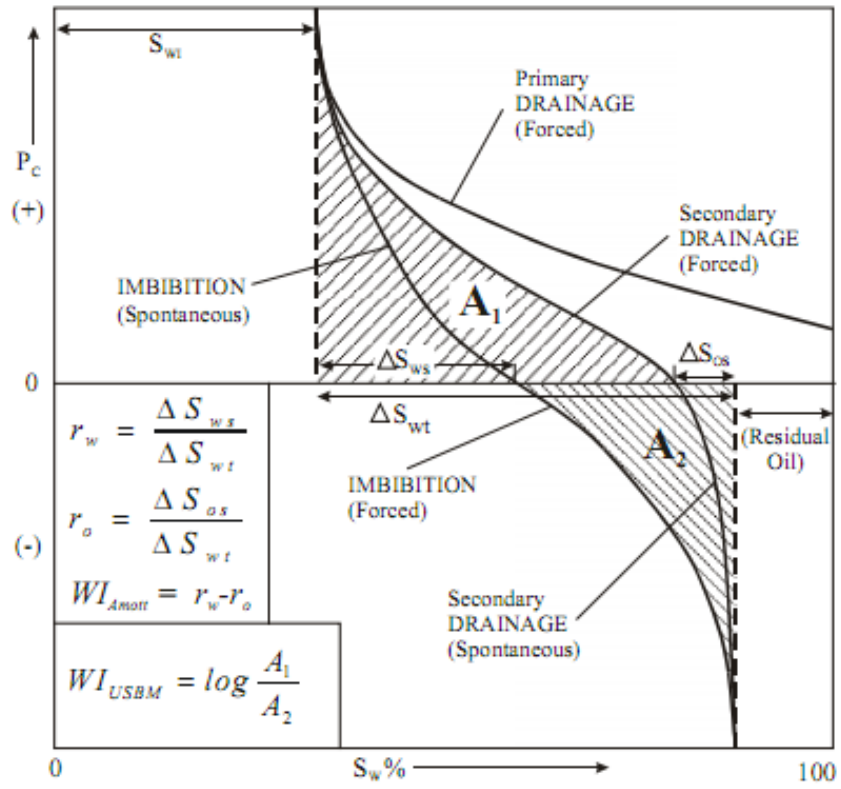

Figure 2.2: Capillary Pressure - Capillary Pressure Curve and the relationship of wettability measurements by Amott Method and USBM test to P_c (12).

2.2 Fluid Properties

2.2.1 Saturation

Oil, water and gas saturations are important parameters in the study of oil and gas reservoirs. Fluid saturations are defined as the ratio of the volume of fluid in a core sample to the pore volume of the sample(12).

$$S_w = \frac{V_w}{V_p}, \quad S_o = \frac{V_o}{V_p}, \quad S_g = \frac{V_g}{V_p} \tag{2.7}$$

Where V_w, V_o and V_g are water, oil and gas volumes, and S_w, S_o, and S_g are water, oil and gas saturations. Fluid saturation are more meaningfull if expressed with the respect to effective porosity, since pore spaces that are not interconnected with each other, not are producible.

$$S_o + S_w + S_g = 1 \tag{2.8}$$

2.2.2 Viscosity

Viscosity is defined as the internal resistance for a fluid to flow.

$$\tau = \mu\gamma \tag{2.9}$$

Where τ is share stress, μ viscosity and γ is the share rate defined as $\frac{dv_x}{d_y}$

Viscosity of fluids varies with temperature and pressure. Most fluids are rather sensitive to changes in temperature, but relatively insensitive to changes in pressure until rather high pressure has been attained. The viscosity of fluids usually rises with pressure at constant temperature. Nevertheless, one exception to this rule exists, water. The viscosity of water decreases with increasing pressure, but for most cases the pressure effect on fluid viscosity can be ignored. Temperature has a different effect on the viscosity of liquids and gases. A decrease in temperature causes the viscosity of a fluid to rise. In addition, the liquid viscosity increases with increasing molecular weight(12).

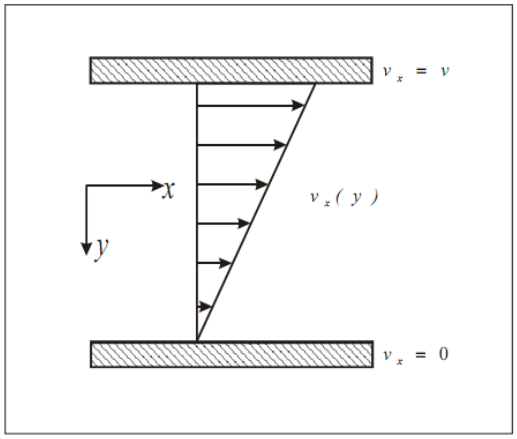

Figure 2.3: Viscosity - Steady-state velocity profile of a fluid entrained between two flat surfaces(12).

2.2.3 Surface and Interfacial Tension

There is a natural tendency for liquids to minimize their surface area. Drops tend to take a spherical shape in order to achieve this. This tendency for a liquid to expose such minimum free surface is called surface tension, and this will cause an increase of internal pressure in order to balance the surface force(15).

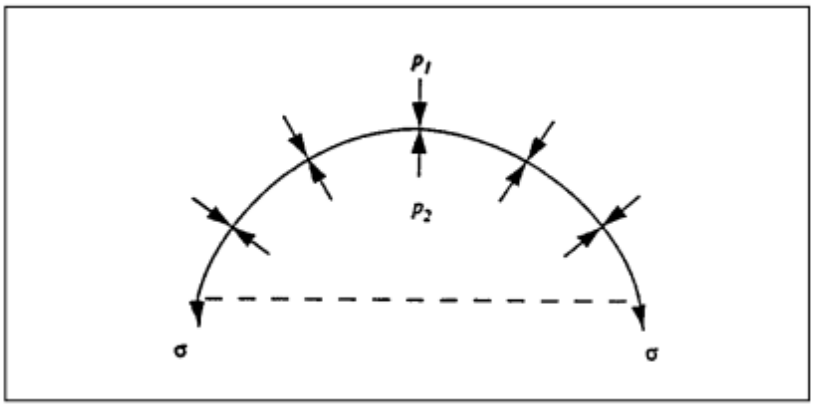

Figure 2.4: Surface Tension - Capillary equilibrium of a spherical gap(12).

The interfacial tension is a similar tendency which exists when two immiscible fluids are in contact. Surface and interfacial tension of fluids result from molecular properties occurring at the surface or interface(12).

2.2.4 Density

Density is defined as the mass of fluid per unit volume. It varies with temperature and pressure, and is measured in kg/m^3. Specific gravity is defined as the ratio of the weight of a volume liquid to the weight of an equal volume of water at the same temperature(12). Density varies a lot by temperature and pressure. Because of this, the units of mass and volume used at the measured temperature must be explicitly stated when reporting the density. The standard reference temperature for international trade in petroleum is 60 ^{o}F and 1 atm(15).

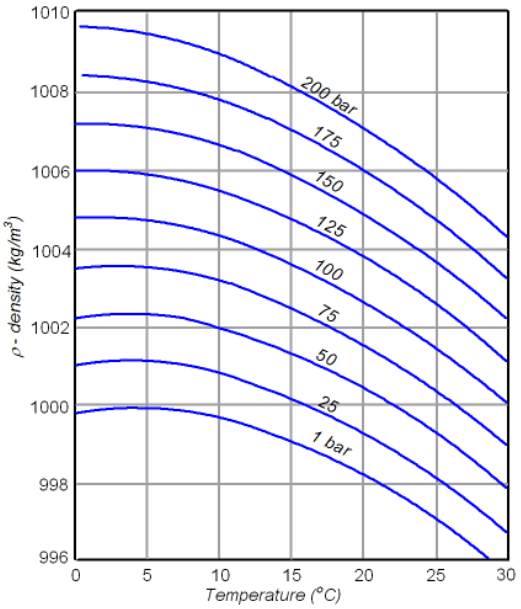

Figure 2.5: Density - Density variations of water with pressure and temperature changes(16).

3

Nanotechnology in the Petroleum Industry

Nanotechnology can contribute in countless areas of oil and gas Exploration and Production (E&P). The ability to be more efficient, less expensive and more environmentally friendly will play a very important role in the years to come. However, many of the opportunities are still only in laboratory and research development. Companies would like to be at the forefront regarding nanotechnology, but reasonable costs compared to oil price are necessary. In this chapter, current challenges faced in the industry, and the potential for solutions based on nanotechnology will be presented.

3.1 Nanotechnology Applications for the Oil Industry

3.1.1 Nanoparticles, Nanofluids and Nanosensors

Nanoparticles, nanofluids and nanosensors are attracting a great deal of interest with their enormous potential to provide enhanced performance properties, their size, and their ability to significantly alternate optical, magnetic and electrical properties. Customized nanoparticles have the ability to enhance oil recovery, improve exploration, and be useful in formation scale control. Nanoparticles can be tailored to alter reservoir properties such as wettability, improve mobility ratio, or control formation fines migration. Nanofluids have successfully been developed in laboratories, and the upcoming challenge is to develop techniques for cost-efficient industrial-scale production of nanofluids. In nearly all cases, the thermal conductivity of conventional heat transfer

of fluids is improved by the addition of small amounts of nanoparticles(17). In addition, development of pressure- and temperature-sensitive nanosensors will enable in-situ measurements within the reservoir(18). Nanosensors can provide improved temperature and pressure ratings in deep wells and hostile environments(6).

3.2 Recent Progress in the Oil Indudstry

3.2.1 Exploration

The need for exploration in even more challenging remote and offshore sites requires revolutionary technical solutions for the oil and gas industry. Developing more sophisticated methods to enhance field characterization techniques and processes can lead to improved oil recovery. The natural field methods utilize the gravitational, magnetic, electrical, and electromagnetic fields. Searching for local perturbations in these naturally occurring fields may be of economic or other interest due to their concealed geological features(19). By improving these survey methods, a better understanding of the reservoir, both its chemical and physical properties, can be achieved, and more oil and gas could be extracted. Many of these current state of art technologies, beside seismic acquisition, only penetrate and provide information a few inches from the wellbore.

As mentioned, many of these techniques lack the required resolution and the capacity to deeply penetrate reservoir lithologies, especially in tight formations. In harsh environment, like high temperature and high pressure, many of the logging tools become unreliable. Reasons can be reduction in quality due to tool failures, and lessening in available downhole sensors(20). By introducing sensors that can migrate under their own power, or with the movement of injected fluids, one may provide an accurate description of the rock and fluid interactions. Micro- and nano-sensors can illuminate the hydrocarbon reservoirs by describing chemical and physical properties of reservoir fluids and rocks beyond the wellbore, three-dimensional distribution of reservoir fluids and rocks, and dynamic paths of fluids(21). Nanomaterials make great tools for the development of these sensors, and the formation of imaging-contrast agents due to their substantial alternation in optical, magnetic, and electrical properties.

Nanomaterials combined with smart fluids can be used as extremely sensitive sensors for pressure, temperature, and stress downhole under harsh conditions(22).

3.2.2 Drilling

Enhancing drilling performances will reduce operational cost and non-productive time. Since the average field size has been declining drastically since the 1960s and 1970s(23), and new discoveries are less frequent, the drilling efficiency becomes more important. Furthermore, the drilling challenges and environmental regulations have increased due to E&P in more and more fragile environments. Drilling in ultra deep water and Arctic areas imposes substantial demands on the operators. Future operations will possibly face challenges due to operation depth, the nature of subsurface geo-hazards with increasing depth, and complexity in drilling operations to mention some(24). To face these problems, the industry is in need of mechanically strong, chemically and physically stable, and physically small materials to be used in nearly all areas of E&P(24).

Synthetic nanoparticles represent the most promising progress of technology in drilling(22). These nanoparticles have exhibited exceptional rheological properties. Advanced drilling fluids based on polymers that are physically and chemically associated with nanoparticles, along with amphiphilic surfactants or polymers have been developed. These fluids have properties that can be altered in response to a change in stimuli, such as temperature, pH and salinity(22). Designed nanoparticles, and especially nanocrystaline materials in combination with advanced drilling fluids, will probably improve the rate of penetration and decrease wear on drilling equipment significantly(22). Nano-based mud additive is expected to improve the thermal conductivity of nanofluids, which consequently will provide more efficient cooling of drill bits, and longer operational cycles.(25). In addition, additives in casing to increase compressive and flexural strength, as well as light-weight rugged structural materials was studied in the project thesis, *The Use of Nanotechnology in the Petroleum Industry*(6).

3.2.3 Production

Completion is one of the most challenging processes of production, since it is important to assure an efficient flow toward the surface. Completion and stimulation fluids are

used in every well and are critical for reservoir productivity and improved flow of hydrocarbons(26). Viscoelastic surfactant fluids have been used as completion fluids in the oil industry as gravel-packing, fracture-packing, and fracturing fluids because of its excellent rheological properties, and maintain low-formation-damage characteristics compared to cross-linked-polymer fluids. Nanotechnology can be used to maintain viscosity of such fluids at high temperature, and controlling the loss of viscoelastic surfactant fluids without generating formation damage(27).

During processing of oil, heavy organic compounds are one of many challenges. The production of bitumen, or other heavy-organic containing hydrocarbons, may be affected by flocculation and deposition of asphaltenes. Dispersed nickel nano- and micro-particles in heavy oil matrixes have made it possible to remove up to 85 % of the asphaltenes in the original solution(28). In addition, a new generation of nano-membranes has been developed for the separation of metal impurities in heavy oil, and impurity gases in tight gas. These membranes may enhance the exploration of tight gas substantially by providing efficient methods for removing impurities(22).

3.2.4 Enhanced Oil Recovery

As the production rate of existing fields start to decline and the frequency of new explorations are significantly lower, increasing the recovery factor is of great importance. Many fields are abandoned with a residual oil saturation of more than 30 %(29). Increasing the recovery factor by few percent may provide billions of dollars in additional profit. Enhanced oil recovery techniques, or tertiary recovery, are designed to increase the oil recovery above secondary recovery base line. Thermal recovery which introduces heat to reduce the viscosity of especially heavy oil, miscible or immiscible gas injection, and chemical injection, which includes the use of polymers, alkali, and surfactants are all tertiary recovery methods(2).

Nanotechnology has the possibility to improve these methods beyond current applications. With ultra-small size and high surface area to volume ratio, nanoparticles have the ability to penetrate pores where conventional recovery methods are unable to. Injecting displacement fluids, such as water, CO_2 or surfactant solution, often possess a lower viscosity than the oil. By adding nanoparticles, the viscosity of the injected fluid can

be increased, and a lower mobility ratio may be achieved. A laboratory study by *Shah and Rusheet* showed that both density and viscosity of CO_2 increased by adding only 1 % CuO nanoparticles. The viscosity of CO_2 nanofluids proved to be 140 times greater than conventional CO_2(30). Some papers also address experiments where combinations of nanoparticles and surfactant solutions are tested. *Le et al.* studied synergistic blends of SiO_2 nanoparticles and surfactants for EOR in high-temperature reservoirs. They performed experiments blending different types of surfactants with SiO_2 nanoparticles. Some of the blends showed great potential for EOR application because of their resistance to adsorption onto the rock surface, and thermostability at 91^oC (31). *Suleimanov et al.* carried out experiments which showed how dispersed nanoparticels in an aqueous phase could modify the interfacial properties of a liquid/liquid system, if their surface were modified by the presence of an ionic surfactant. The application of nanosuspension in their study permitted significant increase in the efficiency of oil displacement flow rate. In homogeneous pore media, oil recovery before water breakthrough was increased by 51 % and 17 % for surfactant aqueous solution with nanoparticle addition respectively to water and surfactant aqueous solution(32).

Polysilicon nanoparticles (PSNP) have been considered as an EOR agent by *Onyekonwu and Ogolo*. One important characteristic of polysilicon nanoparticles is its ability to change rock wettability. *Onyekonwu and Ogolo* discuss three different PSNP which alter the rock wettability in different manners. Their results showed that silane treated NWPN, and HLPN which is treated by a single layer organic compound, had an improvement of over 50 % after primary and secondary recovery on a water-wet rock (33). *Ju and Fan* address the challenges relating to the application of nanopowder in oilfields to enhance water injection by the effect of changing wettability through adsorption on porous walls of sandstone. Their result revealed that wettability of surface sandstone can be changed from oil-wet to water-wet by adsorption of untreated polysilicon nanoparticle, LHPN. Furthermore, the sandstones' effective permeability of water was improved, while a decrease in absolute permeability was observed(34).

Nanoparticles have properties that are potentially useful for certain oil recovery processes, as they are solid and two orders of magnitude smaller than colloidal particles. The nanoparticle stabilized emulsions droplets are small enough to pass typical pores, and

flow through the reservoir rock without much retention(35). Spherical fumed silica particles with a diameter in the range of several to tens of nanometers are the most commonly used. Their wettability is controlled by the coating extent of silanol groups on the surface, and are considered to be hydrophilic if over 90 % of the surface is covered by silanol groups. With these hydrophilic properties, they will consequently form a stable oil-in-water emulsion. Conversely, if the silica particles are coated with only 10 % of silanol groups on the surface, they are hydrophobic, and will form a water-in-oil emulsion(35). Nanoemulsions are very stable over time, and resistant to coalescene and the exchange of the dispersed phase between droplets(2). The particles are also able to stabilize supercritical CO_2-in-water emulsion(36) and water-in-supercritical CO_2 emulsion(37).

Even though nanoparticles in many cases show encouraging results through their applications, the quantity and size of the particles are vital. *Kanj et al.* identified the usable size of nanoparticles in reservoir rocks, and validated their transport potential(38). Another study performed by *Skauge et al.* concludes that silica particles propagate easily through a pore system, and due to their natural occurrence in the reservoir, they pose no harm to the environment. They also seem to be too small to strain or block pores, which make them of great interest for EOR purposes(39).

The potential for using nanotechnology in EOR is enormous. The technology has been widely used in several other industries, and the interest in the oil industry is increasing. Silica nanoparticles are the most widely tested, and have shown good EOR applications. Recently, studies have explored the potential of Al_2O_3, MgO, Fe_2O_3 in addition to SiO_2 nanoparticles. The results showed that some combinations have yielded better results than SiO_2(40). Based on the current knowledge, it is expected that both chemical EOR and specifically micellar flooding will make huge benefits from nanotechnology and nano-emulsion in particular in the future(41).

3.2.5 Environmental and Occupational Issues

While the production and use of engineered nanostructured particles is an essential part of the "nanotechnology revolution", the safe and responsible use of such particles present several challenges(42). Research and evaluation is needed to create a shared

understanding and sufficient knowledge of nanotechnology development and risk management issues that must be addressed(43). It is important that the oil and gas industry leverage lessons and best practices from other industries that are utilizing nanotechnology. By doing this, the oil and gas industry can enhance their understanding of the environmental and occupational safety and health implications of nanotechnology(44).

On the other hand, nanoparticles represent a new generation of environmental remediation technologies that could help solve some of the most challenging environmental problems. Nanoscale iron particles can be very effective for the transportation and detoxification of different common environmental containments, as chlorinated organic solvent and PCBs (45).

This improvement concerning handling of environmental hazards can make it easier to get public and politic acceptation for oil and gas E&P, especially in fragile areas. Even though nanotechnology in some areas can help to remedy these problems, the importance of understanding and accepting the health and safety challenges is essential. Making the handling of environmental containments easier, more effective, and more economical profitable is valuable, as long as it can be proven to be risk-free.

4

Nanoparticle Effect on Reservoir Properties

Formation damage is an undesirable operational and economical problem that can occur during the various phases of oil and gas recovery from subsurface reservoirs, including production, drilling, hydraulic fracturing, and workover operations. Formation damage can be caused by different unfavorable processes including chemical, physical, biological, and thermal interactions of formation and fluids. The indicators of formation damage include permeability impairment, skin damage, and deformation of formation under stress and fluid shear(46). Once injecting particles of nanometer size, retention in porous media can damage formation properties, and is one of the major issues regarding nanoparticle transport.

4.1 Retention in Porous Media

Porous media is a complex structure of pore bodies and throats covering a range of sizes. Particle retention in porous media has been a concern for many industries, since the transport of particles is limited to the degree to which the particles are retained by the porous medium. Reservoir rocks that bear oil and gas can be severely affected by particle invasion(47).

Particle movement in porous media is a very complex process due to complexity and forces controlling solid movement in porous media. Many authors have addressed these

problems, and three main mechanisms are mentioned in the literature. Adsorption of particles onto rock surface because of the Brownian motion, and the electrostatic interaction between the migration particles and the solid surface of the pores is one of the mechanisms(47). Mechanical entrapment, or deep-bed filtration, in small pores has been recognized as another element of retention(48). The mechanism, also known as straining, leads to blocking of narrow pore throats by larger particles. The evidence for mechanical entrapment is taken to be either that the particle concentration in the effluent does not reach the injected concentration, or that it would do so only after injecting a large volume of particles (39).

The third entrapment mechanism is known as log-jamming. This mechanism is similar to straining, but particles can block pores larger than the particle size. Due to density differences between moving particles and carrying fluid, sedimentation or gravity settling will take place. When pore throats narrows, flow velocity will increase. Water molecules will then accelerate faster than heavier particles, and accumulation will occur. Due to gravity settling the pore throat will gradually be reduced and eventually blocked. The main factors governing the log–jamming effect are particle concentration and effective hydrodynamic size, pore size distribution and flow rate(47),(49).

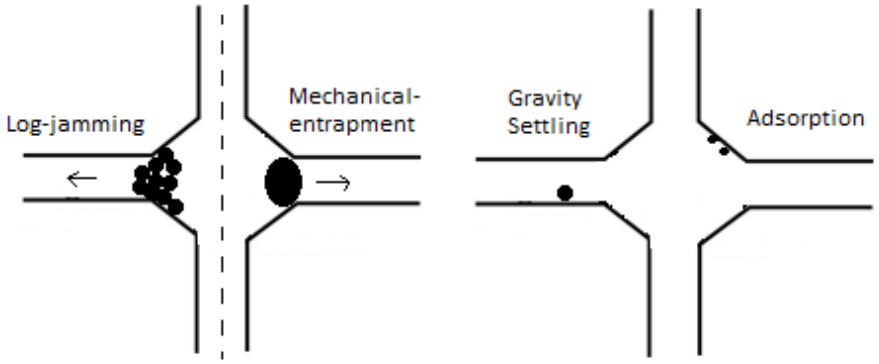

Figure 4.1: Entrapment Mechanisms - Four different entrapment mechanisms; log-jamming, mechanical entrapment, gravity settling and adsorption.

These mechanisms are to be considered when injecting nanoparticles or other agents in a porous media. Blocking of pores can damage the reservoir, change the flow pattern and reduce the permeability. Although in some cases, blocking agents have been applied to the reservoir to prevent channeling of fluids through high permeable zones(50). For most EOR methods, the agents used have a different target than blocking pores or fractures. Blocking pores and reducing permeability are therefore not desirable, and several parameters affect the degree of blocking. Flow rate, fluid viscosity, particle concentration, pH and ionic strength all have certain effects on the permeability decline. Experiments have shown that low fluid velocity and large particle size lead to shallow and severe damage, while higher concentration leads to more severe permeability damage(47).

4.2 Effect on Permeability and Porosity due to Adsorption of Nanoparticles

Authors have presented experimental and mathematical models regarding changes in reservoir properties due to adsorption of nanoparticles. *Ju et al.* have studied the wettability and permeability changes caused by adsorption of nanometer particles onto rock surfaces. They have evaluated the changes of porosity and absolute permeability caused by particle injection. Instantaneous porosity is expressed by equation 4.1

$$\phi = \phi_0 - \Sigma\Delta\phi \tag{4.1}$$

Where $\Sigma\Delta\phi$ is the variation in porosity, caused by retention of nanoparticles.

In addition, a modification of Xianghui and Faruk Civan's model for permeability is presented as an expression for instantaneous permeability.

$$K = K_0[(1-f)k_f + \frac{f\phi}{\phi_0}]^n \tag{4.2}$$

K_0 and ϕ_0 are initial permeability and porosity, while K and ϕ are existing local permeability and porosity. k_f is given as a constant for fluid seepage allowed by the plugged cores, and f is a flow efficiency factor of cross-section area open to flow(5).

Ju et al. also present an evaluation of relative permeability alternation caused by nanoparticle injection. It is known, as mentioned in Section 3.2.4, that nanoparticles that spread on rock surfaces can alter the wettability of a rock. Wettability is one of the most important parameters to determine relative permeability of a porous media. Assume a given volume, V, of one type of nanoparticle trapped in pore space. If supposing spherical particles with equal diameter touching each other at one point, and using real volume of particles as the dominator, the specific area can be defined as

$$s_b = \frac{A}{V} = \frac{n^3 d^2 \pi}{\frac{1}{6} n^3 d^3 \pi} = \frac{6}{d} \tag{4.3}$$

If further assuming that v is the volume of particles adsorbed on the pore surface, and v^* is the volume of particles entrapped at pore throats per unit bulk volume of the media, in addition to supposing that adsorption is first developed as a single layer, the total surface area in contact of fluids per bulk volume of the porous media is calculated by

$$s = \beta(v - v^*)s_b \tag{4.4}$$

where β is the surface area coefficient. The specific area of sand core can be calculated by an emperical formula

$$s_v = 7000\phi\sqrt{\frac{\phi}{K}} \tag{4.5}$$

At the time s $\geq s_v$, the total surface per unit bulk volume of the porous media is completely covered by particles that have been adsorbed on pore surfaces or entrapped at pore throats. At this point, wettability is determined by nanoparticle properties. Continued, further deposition of particles will only lead to reduction in porosity and permeability(5). Before injection of nanoparticles, the relative permeability to oil and water are given as K_{ro} and K_{rw}. If the surface per unit bulk volume of a porous media is not completely occupied by nanoparticles, the relative permeability of oil and water are to be considered as a linear function of the surfaces covered by nanoparticles(5). Then the relative permeability of oil and water will change gradually in relation to the area covered by particles.

With this evaluation as a background, *Ju and Fan* later performed both experimental and numerical studies on porosity and permeability changes caused by nanoparticle flooding. Their results show that both ratios (K/K_0 and ϕ/ϕ_0) are declining with

increasing volume nanofluid injected, where K_o is initial permeability and ϕ_o is initial porosity. Also, numerical solutions show that porosity and permeability ratios are smaller close to the inlet than to the outlet. Both rations are functions of dimensionless distance, and are increasing gradually toward the initial value when dimensionless distance approaches 1. These results imply that nanoparticle adsorption at pore walls, and pore throat blocking, occur at a higher frequency closer to the inlet(34).

4.3 Wettability Alternation and Surface Wetting

As stated in Section 3.2.4, different types of nanoparticles can alter the wettability depending on their surface coating. Most of the particles that have been examined to this day are polysilicon nanoparticles. Three different types of polysilicon nanoparticles can change the wettability of a rock surface differently. The untreated polysilicon nanoparticle, LHPN, can turn an already water-wet rock strongly water-wet, or make an oil-wet rock water-wet. HLPN is treated with single layer organic compound, and can render a water-wet rock oil-wet, or make an already oil-wet rock strongly oil-wet. While NWNP is treated with silane, and can achieve intermediate wetness by making a rock either strongly oil-wet and strongly water-wet at the same time, or make the rock neither oil- or water-wet(33). For these different types of polysilicon nanoparticles to change the wettability of a rock surface, they need to adhere and spread over the surface. For optimal distribution, factors such as concentration and particle size are important. The degree of dispersion plays an important role in the change of contact angle and wettability, and has been widely addressed by various authors..

Vafaei et al. look at the effect of nanoparticles on sessile droplet contact angle. The study indicates that the concentration and size of nanoparticles in solution have an important role in the variation of the droplet contact angle(51). With increasing concentration, the contact angle is increasing linearly for the same droplet volume until it reaches a peak, before decreasing with increasing concentration. Observations from the study also show that smaller nanoparticles were more effective in raising the contact angle(51). *Sefiane et al.* suggest that that improvement in contact line motion affected by the presence of a nanoparticle solution may have two potential underlying mechanisms. The mechanisms could be either enhancement caused by

structural disjoining pressure, or enhancement due to nanoparticle adsorption on the surface(52). *Wasan et al.* studied the role of disjoining pressure for wetting and spreading of nanofluids on a solid surface. Disjoining pressure is a pressure that arises when two surface layers reciprocally overlap, and is caused by the total effect of forces that are different by nature. Electrostatic forces, the forces of "elastic" resistance of solvated, or adsorbed solvated, films, and the forces of molecular interaction can act as components of the disjoining pressure(53).

Wasan et al. reported that the driving force for the spreading of a nanofluid is the structural disjoining pressure direct towards the wedge from the bulk solution. The film tension is high near the vertex, because the particles are structuring in the wedge confinement. As the tension on the film gets bigger towards the top of the wedge, it will cause the nanofluid to spread at the wedge tip. This will improve the dynamic spreading behavior of the nanofluid(54). Figure 4.3 shows how nanoparticles structure inside the wedge film, formed between an oil droplet and a solid surface. The result is that the nanoparticles exert a large pressure through the wedge film relative to the bulk solution. This excess pressure, also called disjoining pressure, will separate the two phases from each other(54).

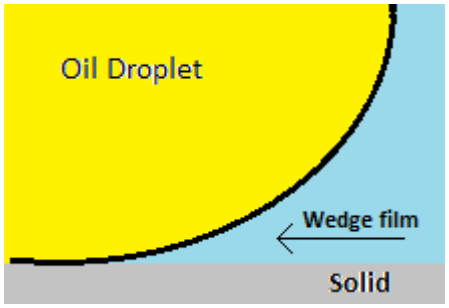

Figure 4.2: Oil drop placed on a solid surface (54).

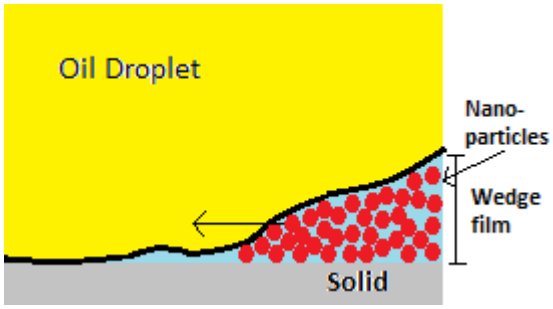

Figure 4.3: Nanoparticle structuring in the wedge-film, resulting in structural disjoining pressure at the wedge vertex(54).

5

Experimental Procedure

5.1 Cleaning and Measurement of Core Properteis

The laboratory experiments were performed on Berea Sandstone cores delivered by IRIS in Stavanger. Berea Sandstone is a sedimentary rock whose grains are predominantly sand-sized and are composed of quartz sand held together with silica. The sandstone has relatively high porosity and permeability, which makes it a good reservoir rock(55).

5.1.1 Soxhlet Extraction

The cores were relatively clean and dry when they arrived from IRIS, but extraction using Soxhlet apparatus were still conducted. Soxhlet is one of the most widely used cleaning methods, and is primarily used in laboratories. Toluene, or in the case of relatively clean cores, methanol is heated to a slow boil in a Pyrex flask. The methanol has a boiling point at 65 ^{o}C(56), and the vapor will move upwards and engulf the core. If the core is contaminated by oil, toluene must be applied. Toluene has a much higher boiling point than methanol and any water within the core sample in the thimble will be vaporized. Toluene and water, or methanol vapor, will enter the inner chamber of the condenser and condense as a result of cold water circulating. The liquefied toluene will fall from the condenser onto the core in the thimble, and further soak the core and dissolve any oil present. If no oil is present, methanol is applied. The vapor will condense in the same manner and dissolve any contaminations. When either the toluene or methanol level within the Soxhlet tube reaches the top of the siphon tube arrangement, the liquids will flow into the boiling flask due to a siphon effect. The

extracted fluids and contaminations are then collected in the boiling flask, and another cycle of cleaning can be performed(12).

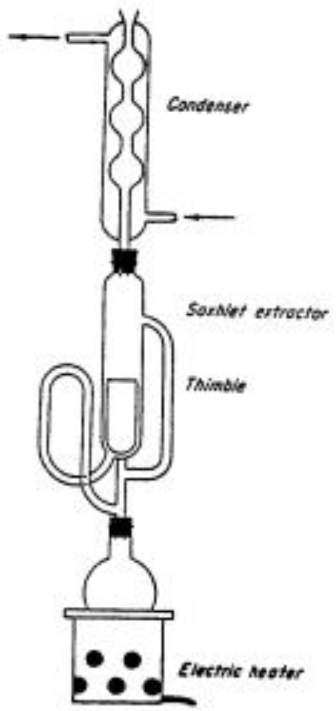

Figure 5.1: Soxhlet Apparatus - Schematic Diagram of Soxhlet Apparatus (12).

The duration of Soxhlet extraction can vary from hours to several weeks, depending on eq. the composition of the oil or the permeability of the rock. Further, the samples were placed in a desiccator-cabinet to remove humidity.

5.1.2 Porosity Measurements

The method used for measuring effective porosity is the helium technique. The helium porosimeter uses the principle of gas expansion.
The use of helium has several advantages(12):

- Helium particles are small and can penetrate small pores.
- It is an inert gas and does not adsorb on rock surfaces as air may do.

- Helium can be considered as an ideal gas for pressures and temperatures usually employed in the test.

- Helium has high diffusivity and therefore affords a useful means of determining porosity of low permeability rocks.

First the diameter and length of each core was measured for bulk volume calculations. Step two was to measure a reference volume, as seen in Figure 5.2. The helium porosity apparatus was applied with a helium supply of 10 bar, and reference volume V_2 was measured. Further, V_1 for each matrix cup containing the cores were measured. Combining the information in Table A.1, the effective porosity for each core can be calculated from Equation 5.1.

$$\phi_e = \frac{V_b - V_k}{V_b} \tag{5.1}$$

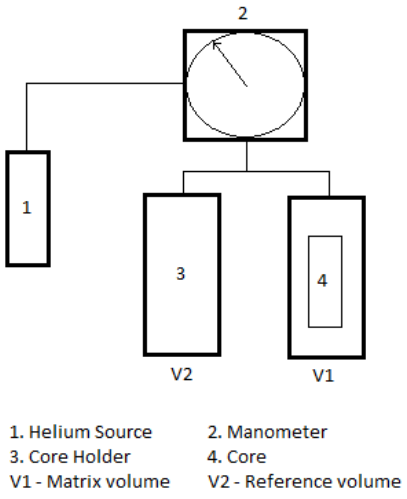

Figure 5.2: Porosity Apparatus - Schematic of apparatus used to porosity by helium method.

5.1.3 Air Permeability Measurements

Determining the gas permeability was done by using a constant head parameter as shown in Figure 5.3. This equipment is designed for plug or whole core permeability measurement. The clean and dry core was placed inside the core holder. A sleeve pressure of approximately 20 bar was applied. Upstream and downstream pressures are measured by manometers on both sides of the core, and air flow is measured by means of a calibrated outlet. Different injection pressures with the same varying pressure drop from inlet to outlet were tested. Pressure and flow rate were measured, and gas permeability was calculated using Equation 5.2.

$$k = \frac{Q_{atm}\mu L 2 P_{atm}}{A({P_1}^2 - {P_2}^2)} \tag{5.2}$$

This information was used to make Klinkenberg plots and find the absolute permeability.

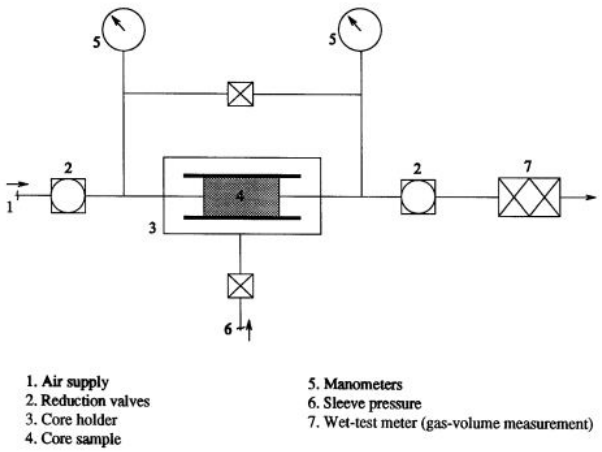

Figure 5.3: Constant Head Parameter - Schematic of apparatus used to measure gas permeability (12).

5.2 Fluid Properties

5.2.1 Formation Brine

Different compositions of brine were prepared, 0,3 wt%, 3 wt% and 10 wt% NaCl. The NaCl was mixed with distilled water and stirred to make sure that all salts were completely dissolved. For all flooding experiments, saturation of cores, and dissolving nanoparticles, 3 wt% brine was applied.

5.2.2 Oil

The oil used in the experiments was kerosene, a type of paraffin oil. The oil was delivered by UNITOR Chemicals AS. The oil is a clear liquid formed from hydrocarbons. Kerosene is a lighter oil, which can be obtained either from the distillation of crude oil under atmospheric pressure, or from catalytic, thermal or steam cracking of heavier petroleum steams. It consist of mainly carbon chains containing between 6-16 carbon atoms per molecule, like eq. alkyl benzenes and alkylnaphthalenes(57)

5.2.3 Nanoparticles

The particles used in this thesis are SiO_2 nanoparticles. Three different types of hydrophilic silica nanopowder were delivered by Evonik Industries and Elkem Silicon Materials. They had a specific surface area ranging from 50 to 300 m^3/g, and an average particle size from 7 to 100 nm. The three different types were Elkem 999, Aerosil 130 and Aerosil 300.

Product name	Producer	Specific Surface Area	Average particle size
		[m2/g]	[nm]
Elkem 999	Elkem	50	100
Aerosil 130	Evonik	130	16
Aerosil 300	Evonik	300	7

Table 5.1: The three different types of nanoparticles examined.

5.2.4 Nanofluid

Nanofluids were prepared by dispersing silica nanoparticles in 3 wt% brine. First, a stability analysis of the three different particles in Section 5.2.3 were conducted. Each type was prepared in a 1 wt% nanoparticle solution. The solutions were mixed using a magnetic stirrer, before being synthesized using an ultrasonic reactor for 3-4 minutes to assure complete dissolution. The solutions were stored for several hours, and the solution of Aerosil 300 proved to be the most stable. These are the particles that have the highest surface area to volume ratio, as well as the smallest average particle size. Aerosil 300 was therefore chosen for further experiments.

5.2.4.1 Viscosity, Density & pH

Determination of viscosity for different nanofluids with varying nanoparticle concentration and salinity was conducted using an Ostwald viscometer. The viscosity is deduced from the comparison of the time required for a given volume of the tested liquid, and of a reference liquid, to flow through a given capillary tube under specified initial head conditions(12). Three nanofluids with different concentrations of nanoparticles, 0,1 wt%, 0,5 wt% and 1 wt%, were tested. Each concentration was mixed with brine of varying salinity. The salinities prepared were 0,1 wt%, 1 wt% and 10 wt%. Based on previous stability analysis, Aerosil 300 was applied.

Density was measured using a pycnometer which is an accurate made flask. The pycnometer is filled with a known volume of a liquid, and the weight divided by this volume results in density. Density measurements were performed on the same combinations of salinity and nanoparticle concentration as viscosity measurements.

pH-measurements were performed using an 827 pH Lab produced by METROHM. This is an accurate apparatus for measurement of pH, and was also applied to all solutions.

5.3 Preparing Cores for Flooding

5.3.1 Saturation with Brine by Vacuum Pump

When rock properties had been measured and calculated, core samples were saturated with 3 wt% brine. The core samples were placed inside the vacuum-container as seen in Figure 5.4, until an under–pressure of approximately 100 mbar was reached. This under-pressure extracted all fluids from the pore system. The cores where then soaked with brine for about one hour, to assure complete saturation.

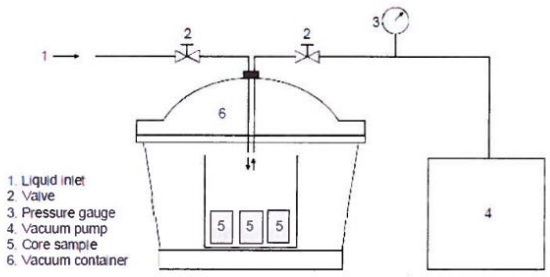

Figure 5.4: Vacuum Pump - Illustration of vacuum pump used in saturation of cores(58).

5.3.2 Liquid Permeability Measurements

Permeability measurements were performed to determine the liquid permeability to each core. Permeability differences before and after injection of nanofluid were also examined. Each core was placed inside a Hassler core holder, and a sleeve pressure of 20 bar was applied. Knauer Smartline Pump 1000, which is a piston pump, provided a constant flow of brine through the core. Pressure was recorded using a Keller PD-33X pressure gauge, measuring pressure in 10^{-3}bar. Brine was flooded through each core at different rates, and pressure differences between inlet and outlet were recorded. Continued, different amount and concentrations of Aerosil 300 nanofluid was flooded through the core at constant rate. Pressure was recorded during nanoparticle flooding. Finally, flow with brine was continued at the same rates as before injection of nano-particles. Pressure was again recorded, and permeability both before and after flooding with nanofluid was calculated using Darcy Equation 2.2, where viscosity of water is 1,02 cP. Only one cycle was performed on each core sample.

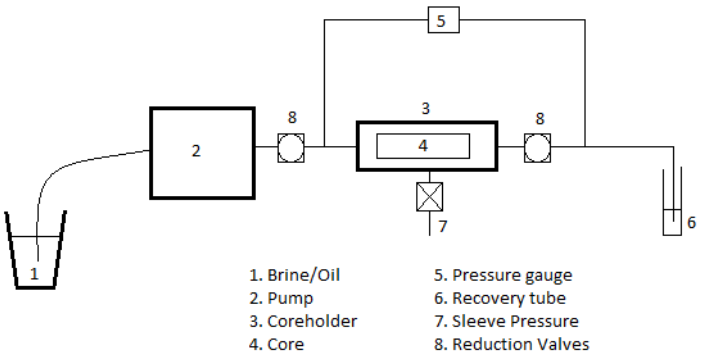

Figure 5.5: Flowing Apparatus - Schematic of apparatus used to flow cores with brine for permeability measurements.

5.4 Establishing Irreducible Water Saturation

After saturation as explained in Section 5.3.1, cores were 100 % saturated with water. Using the design in Figure 5.6, with Exxol-D60 as pumping fluid, displacement process where oil is displacing water was initiated. Each core was placed in a Hassler coreholder as described in Section 5.3.2. A rate of 0,5 ml/min at ambient temperature and pressure was applied until no more water was produced. Continued, the rate was increased to 1 ml/min, 2 ml/min and 4 ml/min until no more water was produced. Produced water was recorded and irreducible water saturation was calculated by Equation 5.3.

$$S_{wi} = 1 - \frac{V_{waterproduced}}{V_p} \tag{5.3}$$

where S_{wi} is the irreducible water saturation, $V_{waterproduced}$ is the produced water and V_p is the pore volume.

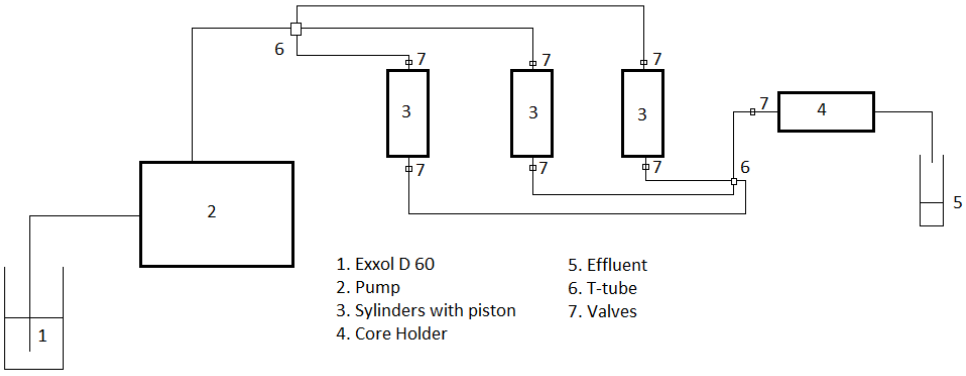

Figure 5.6: Design for flowing of cores - Schematic of apparatus used to flow cores with brine, oil and nanofluid. Each cylinder contains one of the fluids.

5.5 Flooding

Two scenarios were applied for flooding experiments with nanoparticles. The first scenario used nanofluid as a tertiary recovery method. Nanofluid with a concentration of 0,1 wt% was injected after reaching residual oil saturation by brine flooding. The second scenario implemented nanofluid as a secondary recovery method. In this case, brine was replaced by nanofluid from the start, and all oil was displaced by a nanoparticle solution. The setup, Figure 5.6, was used for flooding, and a constant rate of 0,5 ml/min was applied. For scenario number two, oil was initially displaced by brine, until reaching S_{or}. Continued, the cores were cleaned and re-saturated before an identical flooding experiment applying nanoparticle solution as displacing fluid was conducted. Production of oil was recorded and recovery factor was calculated using Equation 5.4, and residual oil saturation was calculated using Equation 5.5.

$$RF = \frac{ProducedOil}{OriginalOilInPlace} = \frac{1 - S_{wi} - S_{or}}{1 - S_{wi}} \tag{5.4}$$

$$S_{or} = 1 - S_{wi} - RF(1 - S_{wi}) \tag{5.5}$$

5.6 Scanning Electron Microscope

Scanning Electron Microscope (SEM) was used to analyze the surface of core samples before and after nanoparticle flooding. Analysis of Aerosil300 nanopowder was also conducted. The microscope was located at the Department of Materials Science and Engineering and was operated by Ph.D. student Suwarno. The microscope used was a Zeiss Supra 55 VP low vacuum SEM. A scanning electron microscope uses a focused beam of high-energy electrons to generate a variety of signals at the surface of solid specimens. The signals that derive from electron-sample interactions reveal information about the sample including external morphology, chemical composition, and crystalline structure and orientation of materials making up the sample(59).

Before analyzing the core samples by SEM-apparatus, the samples needed to be prepared. A maximum height of one inch inside the SEM required either cutting or crushing of the samples. Both methods were performed, in which crushing gave a cleaner rock surface and a better result. The pieces were also covered by a thin carbon layer to assure conductive samples.

6

Results

The results presented in this chapter were obtained through the experimental procedure explained in Chapter 5. All results presented are based on tables included in the Appendix. The porosity and permeability readings for each core sample are presented as bar charts. Experiments performed on permeability impairment measurements were conducted on 9 of a total of 15 core samples, with varying parameters. Some of the 9 core samples used for permeability reduction experiments were brought to SEM-analysis. Finally, six core samples were used for EOR experiments, where two scenarios were tested, and three core samples were applied for each scenario.

6.1 Porosity

The helium porosity measurement gave porosities ranging from 16,6 to 24,5 %. Porosities for the individual core samples are presented in Figure 6.1. Sandstone is predominantly made of quartz sand, but also contains feldspar and clay. The relatively high porosity can be explained by generally sand-sized particles. The size of pore throats are between 0,5 to 5 μm, and the pore chamber is from 5 to 50 μm. The figure is based on results from Table A.1 in Appendix A.1.

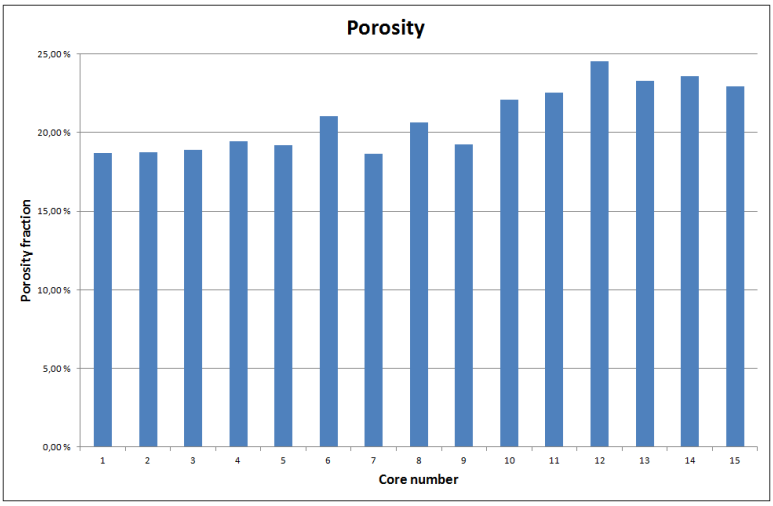

Figure 6.1: Porosity Measurements - Porosity readings for the individual core sample.

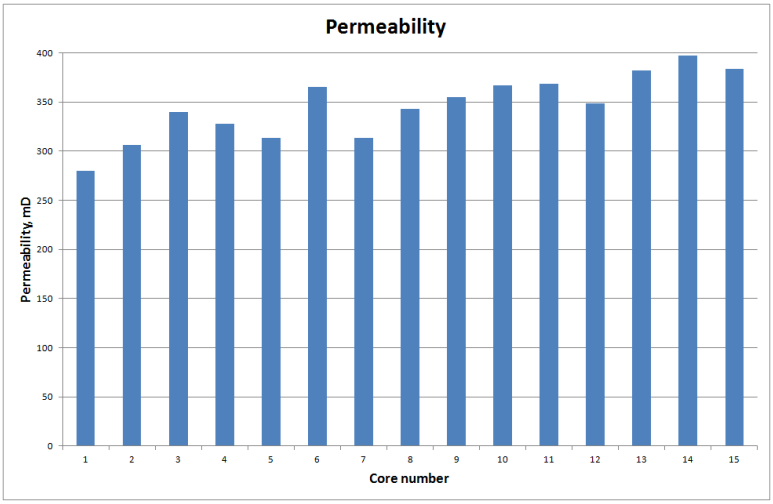

Figure 6.2: Air Permeability Measurement - Permeability readings for the individual core sample.

6.2 Air Permeability

When performing gas permeability measurements, air is used as injection fluid. Air has a viscosity of 0,00179 cP at ambient pressure and temperature. A variety of pressures at the inlet and outlet were applied, and calculation using Darcy's equation was performed. Absolute permeability is found by plotting a Klinkenberg plot for each core sample, as seen in Figure A.1 to A.15 in Appendix A.2.1. The results of air permeability measurements can be seen in Figure 6.2, presented as absolute or liquid permeability. Figures are based on numbers from Table A.2 and A.3 in Appendix A.2.

6.3 Viscosity Measurements

6.3.1 Oil

An Ostwald viscometer was used to determine viscosity of fluids. The oil used in flooding experiment was a type of paraffin oil, kerosene. Kerosene oil has a density of 0,802 g/cm^3, measured with a pycnometer. Two viscosity measurements were performed. The oil had a viscosity of 1,96 cP, and result from the calculation can be seen in Table 6.1.

Fluid	Capilarry Viscometer Data					Density	Dynamic Viscosity
	t1 (s)	k1, mm2/s2	t2 (s)	k2, mm2/s2	µk (average), cSt	g/cc	cp
Koreosene	1005	0,00243	1472	0,00175	2,509075	0,8026	**2,01**
Koreosene	970	0,00243	1357	0,00175	2,365925	0,8026	**1,90**
Average						**0,8026**	**1,96**

Table 6.1: Viscosity calculations for kerosene oil.

6.3.2 Nanofluid

The same procedure as for oil was used to determine the viscosity of nanofluid. A combination of three different salinities with different concentrations of nanoparticles as described in Table 6.2 were examined. For each salinity, the results show that the viscosity increases with increasing nanoparticle concentration, Figure 6.3.

Brine Salinity	Nano concentration	Dynamic Viscosity
wt%	wt%	cP
0,3	0,1	0,998028372
	0,5	1,093875043
	1	1,259937274
3	0,1	1,015319405
	0,5	1,245218813
	1	1,714743551
10	0,1	1,102588968
	0,5	1,119708089
	1	1,48058257

Table 6.2: Viscosity calculations for varying salinity, with three different nanofluid concentrations.

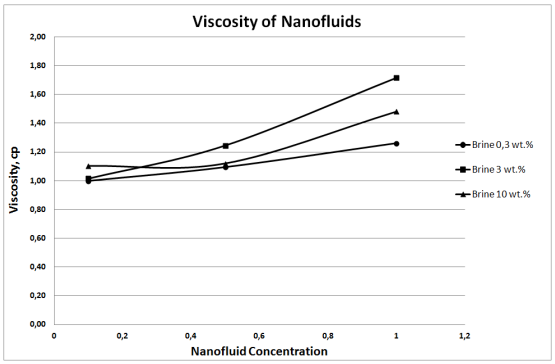

Figure 6.3: Viscosity Measurements - Plot of viscosity versus nanofluid concentration for different salinities.

6.4 Density & pH Measurements of Nanofluids

Density measurements of the combinations described in Table 6.2 show densities around 1 g/cc at ambient pressure and temperature. The tendency of increasing nanofluid concentration shows a slight increase in density. The results obtained using a pycnometer can be seen in Table A.4 in Appendix A.3.

For pH measurements, an 827 pH Lab produced by METROHM was used. pH measurements were performed for each combination of varying salinity and concentration, as already presented. As seen in Figure 6.4, the pH decreases with increasing nanofluid concentration. Brine containing only sodium chloride should not affect the pH with varying salinity as the results show. However, the tendency of decreasing pH with increasing nanofluid concentration is uniform. Figure based on Table A.5 in Appendix A.3.

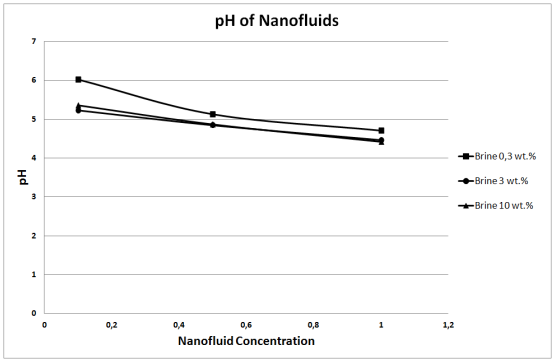

Figure 6.4: pH Measurements - pH vs. nanofluid concentration for different salinities.

6.5 Permeability

6.5.1 Liquid Permeability

The core samples were saturated by a vacuum pump. Liquid permeability measurements were performed on each core, applying the setup shown in Figure 5.5. Different rates were applied, and a very accurate pressure gauge plotted the differential pressure versus time as seen in Figure 6.5. The pump used is a piston pump, and the fluctuations in pressure are caused by this. Darcy equation was used to calculate the liquid permeability for each core, either applying several rates, or one single rate. The results can be seen in Table A.6 in Appendix A.4.

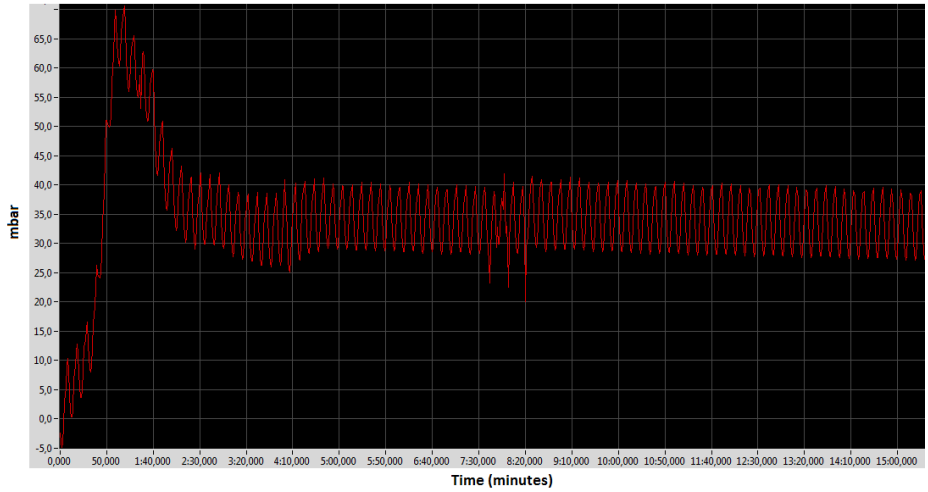

Figure 6.5: Differential Pressure vs. Time - Plot from Keller used for calculation of liquid permeability. Differential pressure in 10^{-3}bar.

6.5.2 Permeability Reduction Experiments

Injecting particles through a core or a reservoir will lead to particle retention in some manner. It can be explained by log-jamming, mechanical entrapment or adsorption onto rock surface as mentioned earlier. In this section, injecting hydrophilic silica nanoparticles through a porous media, and an examination of the effect on permeability is executed. When injecting a solution through a porous medium, permeability impairment or other reduction in reservoir properties should not exceed a desired order of magnitude. The setup shown in Figure 5.5 was used, and a Keller PD-33X pressure gauge was installed to record the differential pressure. Examination of permeability impairment was conducted by comparing the flow ability of brine before and after nanofluid injection. By knowing all parameters, and recording ΔP, Darcy's equation was used to calculate pre and post nanofluid permeability.
To ensure that the setup was working properly, Core #1 was tested with a relatively high concentration. It was injected with a nanofluid concentration of 0,5 wt% for 3 pore volumes, at a rate of 0,5 ml/min. An increase in ΔP was expected due to adsorption or jamming of particles. As observed in Figure 6.6, the pressure was increasing gradually and continuously until 3 PV was injected. This implies that the flow ability through the core has been damaged. By rearranging Darcy's equation, permeability can be calculated from Equation 6.1. When keeping all other parameters than ΔP constant, an increase in differential pressure will result in a lower liquid permeability.

$$k_l = \frac{Q\mu_l L}{A\Delta P} \tag{6.1}$$

Several experiments on nanofluid injection and permeability alternation were performed. The effect of changing different parameters as concentration, rate and volume of solution injected was examined.

6.5.2.1 Effect of Concentration

Based on the increase in differential pressure in Figure 6.6, a concentration of 0,1 wt% was examined for Core #2. Since no pressure was recorded before nanofluid injection on Core #1, it was decided to proceed with 3 PV at an identical rate. As seen in Figure 6.7, the same trend of gradually increasing pressure was observed.

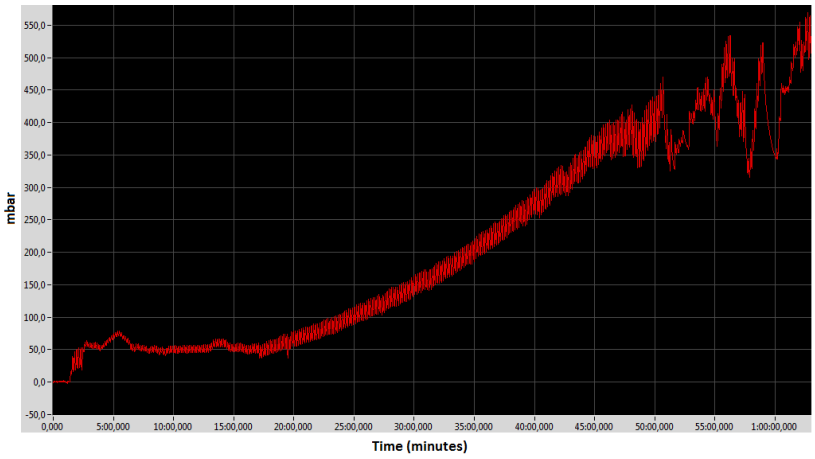

Figure 6.6: Differential Pressure vs. Time - Differential pressure in 10^{-3}bar vs. Time; Injection of 0,5 wt% nanofluid for 3 PV, Core #1.

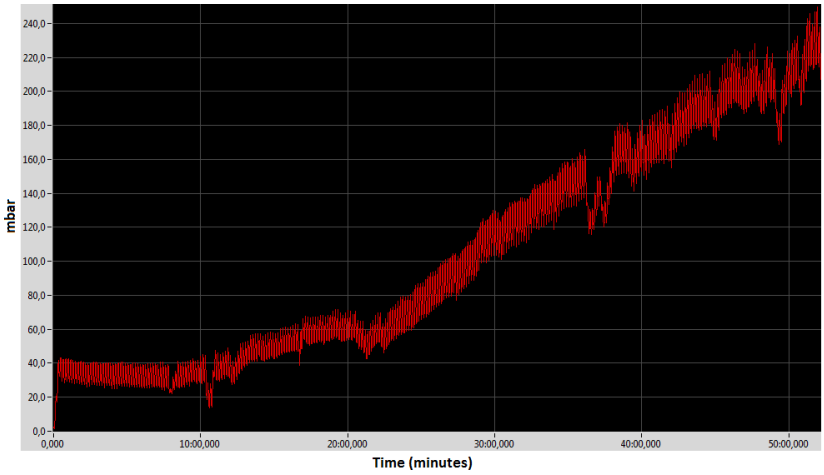

Figure 6.7: Differential Pressure vs. Time - Differential pressure in 10^{-3}bar vs. Time; Injection of 0,1 wt% nanofluid for 3 pore volumes, Core #2.

The differential pressure for brine flooding before nanofluid injection had already been recorded. Brine flooding was continued after nanofluid injection, applying the same rates as before injection of nanoparticle solution. Calculation for Core #2 shows a reduction in permeability of approximately 90 %. The permeability is reduced from around 300 mD, to below 50 mD due to flooding with nanofluid. However, by comparison of Figure 6.6 and Figure 6.7, reducing the concentration from 0,5 wt% to 0,1 wt% give a lower increase in ΔP. In Figure 6.6 the differential pressure increases to over 400 mbar, while in Figure 6.7 the final pressure has only increased to less than 250 mbar. Lower concentration results in lower differential pressure, and thus lower permeability impairment. Nevertheless, the impairment for Core #2 is too high for field application, and both concentration and injection volume were reconsidered.

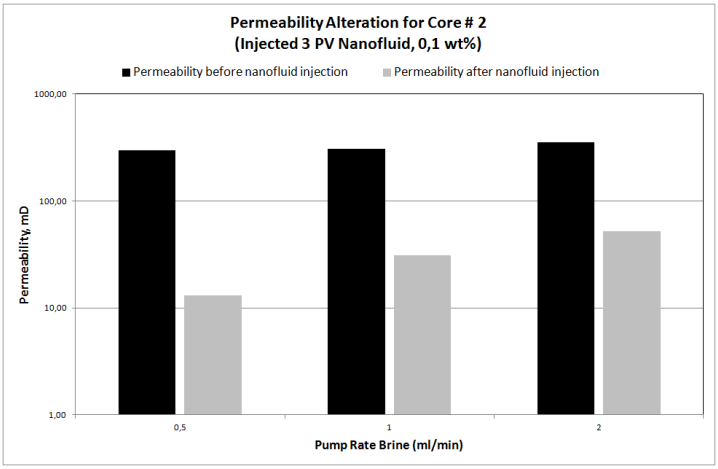

Figure 6.8: Permeability Alternation Core #2 - Permeability when flooding with brine before and after nanofluid injection at semi-log scale.

After reducing rate, injection volume and concentration further, another experiment examining the impact of changing the concentration was performed. It was decided to use a single rate both pre, syn and post nanoparticle flooding. In addition, a much smaller volume of nanoparticle solution was injected, only 0,2 PV. As seen from Figure 6.9, increasing the concentration from 0,01 wt% for Core #8, to 0,05 wt% for Core #9, clearly affects the permeability reduction. However, the permeability impairments are only in a range of 5-15 % for both cores. These results are much more promising

than results obtained earlier. All results show that changing the concentration is undoubtedly an important parameter. Based on the trends in Figure 6.6 and 6.7, and the results in Table 6.3, a lower concentration is necessary to not damage the reservoir properties to a too large extent. All results can be seen in Table A.7 in Appendix A.5.

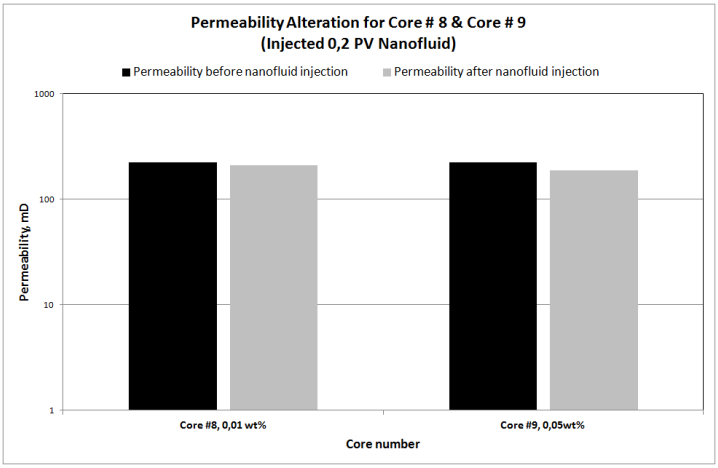

Figure 6.9: Permeability Alternation Core #8 & Core #9 - Permeability impairment for two different concentrations, 0,01 wt% in Core #8 and 0,05 wt% in Core #9.

Core number	Vp	Nanofluid	Rate water	ΔP(Pre)	kabs	Rate Nano	Inj Nano	Rate water	ΔP (Post)	kabs	K reduced
	[cc]	wt%	[ml/min]	[mbar]	[mD]	[ml/min]	[ml]	[ml/min]	[mbar]	[mD]	[%]
8	11,34	0,01	0,1	3,2	223,15	0,1	2,27	0,1	3,4	210,02	**5,9 %**
9	10,56	0,05	0,1	3,2	224,67	0,1	2,11	0,1	3,8	189,20	**15,8 %**

Table 6.3: Permeability reduction after nanofluid injection, concentration changed from 0,01 wt% to 0,05 wt% for Core #8 and Core #9 respectively.

6.5.2.2 Effect of Rate

Particle retention is often affected by rate. Higher velocity in narrow areas can cause heavier particles to accumulate and retain, or in worst case block pore throats. By keeping all other parameters than rate constant, examination of varying rate could be performed. Injection of nanofluid with a concentration of 0,01 wt% for 0,5 PV was

performed on Core #3 and Core #4. The rate was set to 0,5 ml/min for Core #3, and 0,1 ml/min for Core #4. The rates before and after nanofluid injection are identical for both cores. As seen in Table 6.4, changing the rate from 0,5 ml/min to 0,1 ml/min affect the magnitude of reduction positively.

Core number	Vp	Nanofluid	Rate water	ΔP(Pre)	kabs	Rate Nano	Inj Nano	Rate water	ΔP (Post)	kabs	K reduced
	[cc]	wt%	[ml/min]	[mbar]	[mD]	[ml/min]	[ml]	[ml/min]	[mbar]	[mD]	[%]
3	11,37	0,01	0,5	8,00	449,21	0,5	5,20	0,5	51,00	70,46	**84,3 %**
			1	20,00	359,37			1	60,39	119,02	**66,9 %**
			2	40,50	354,93			2	68,99	208,35	**41,3 %**
4	11,38	0,01	0,5	11,50	312,23	0,1	5,31	0,5	15,00	239,38	**23,3 %**
			1	19,50	368,27			1	25,00	287,25	**22,0 %**
			2	31,50	455,96			2	36,00	398,96	**12,5 %**

Table 6.4: Permeability reduction after nanofluid injection, rate reduced from 0,5 ml/min to 0,1 ml/min for Core #3 and Core #4 respectively.

6.5.2.3 Effect of PV Injected

As already observed from Figure 6.6 and 6.7, several pore volumes increase the ΔP to a too great extent. It was therefore desirable to examine the effect of lower injection volumes. Core #4 and #5 were injected with 0,5 PV and 0,2 PV respectively. As seen from Table 6.5, a lower PV does not affect the reduction in a positive way. Decrease in injection volume results in a increase in permeability impairment.

Core number	Vp	Nanofluid	Rate water	ΔP(Pre)	kabs	Rate Nano	Inj Nano	Rate water	ΔP (Post)	kabs	K reduced
	[cc]	wt%	[ml/min]	[mbar]	[mD]	[ml/min]	[ml]	[ml/min]	[mbar]	[mD]	[%]
4	10,63	0,01	0,5	11,50	312,23	0,1	5,31	0,5	15,00	239,38	**23,3 %**
			1	19,50	368,27			1	25,00	287,25	**22,0 %**
			2	31,50	455,96			2	36,00	398,96	**12,5 %**
5	10,46	0,01	0,5	10,00	358,70	0,1	2,09	0,5	20,00	179,35	**50,0 %**
			1	23,00	311,91			1	37,50	191,30	**38,7 %**
			2	45,00	318,84			2	60,00	239,13	**25,0 %**

Table 6.5: Permeability reduction after nanofluid injection, PV injected changed from 0,5 PV to 0,2 PV for Core #4 and Core #5 respectively.

Another flooding was performed examining the effect of minimizing the volume injected. Core #6 and Core #7 was injected with a 0,01 wt% solution for 0,2 PV and

1 PV respectively. Table 6.6 shows an increase from 4,8 % to 12,1 % in impairment when increasing the PV injected. The results obtained for the two comparisons are contradictory. Yet, both comparisons show permeability impairment as a result of nanofluid injection.

Core number	Vp	Nanofluid	Rate water	ΔP(Pre)	kabs	Rate Nano	Inj Nano	Rate water	ΔP (Post)	kabs	K reduced
	[cc]	wt%	[ml/min]	[mbar]	[mD]	[ml/min]	[ml]	[ml/min]	[mbar]	[mD]	[%]
6	11,65	0,01	0,1	4,0	181,38	0,1	2,33	0,1	4,20	172,74	**4,8 %**
7	9,05	0,01	0,1	5,1	124,49	0,1	9,05	0,1	5,8	109,47	**12,1 %**

Table 6.6: Permeability reduction after nanofluid injection, PV injected changed from 1 PV for Core #7 to 0,2 PV for Core #6.

6.5.2.4 Effect of Filtering

Nanoparticles have a tendency to cluster together, which can result in clusters with a much larger size than a single nanoparticle. Blocking of pore throats can be a consequence of these clusters, and filtering was performed to examine this potential. Filtering of nanofluid was done through a 25 nm filter paper. Two cores were then flooded with this solution, originally containing 0,01 wt%. As seen in Figure 6.10, there are small differences between permeability reduction for filtered and not filtered flooding.

It is likely that if clusters are present, those larger than 25 nm will be removed. The process of filtering is however time-consuming, and the results obtained do not differ much from un-filtered core flooding. Both Core #6 and Core#8 are injected with 0,2 PV and 0,01 wt% nanoparticle solution, with and without filtering respectively. For Core #8 a permeability impairment of 5,9 % was observed, while for the filtered case, Core #6, an impairment of 4,8 % was observed. This difference in reduction in permeability is almost negligible, and it can be expected that it could be caused by error margins or other mechanisms.

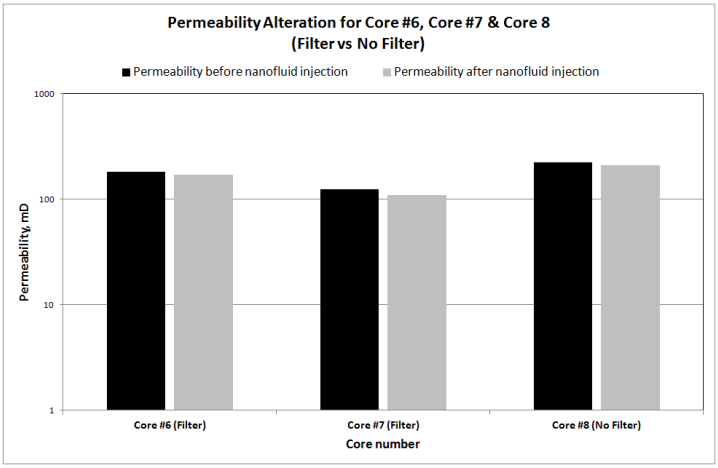

Figure 6.10: Permeability Alternation for Core #6, Core #7 & Core #8 - Permeability impairment using filtered solution vs. no filtered solution. Concentration identical, while PV injected equal 0,2 for Core #6 & #8 and 1 for Core #7

Core number	Vp	Nanofluid	Rate water	ΔP(Pre)	kabs	Rate Nano	Inj Nano	Rate water	ΔP (Post)	kabs	K reduced
	[cc]	wt%	[ml/min]	[mbar]	[mD]	[ml/min]	[ml]	[ml/min]	[mbar]	[mD]	[%]
6	11,65	0,01	0,1	4,0	181,38	0,1	2,33	0,1	4,20	172,74	**4,8 %**
7	9,05	0,01	0,1	5,1	124,49	0,1	9,05	0,1	5,8	109,47	**12,1 %**
8	11,34	0,01	0,1	3,2	223,15	0,1	2,27	0,1	3,4	210,02	**5,9 %**

Table 6.7: Permeability reduction for filtered solution (Core #6 & #7) and no filtered solution (Core #8).

6.5.3 Differential Pressure after Injection of Nanofluid

When performing brine flooding post nanofluid flooding, a continuous decrease in ΔP was observed in some cases. As seen in Figure 6.11, the differential pressure slightly decreased with time. Figure 6.11 shows the differential pressure for Core #2, when brine is injected with a rate of 1 ml/min. The continuous decrease in ΔP may indicate deportation of nanoparticles. Figure 6.12 shows the differential pressure for brine flooding after nanofluid injection for Core #5, applying three different rates, 0,5 ml/min, 1 ml/min and 2 ml/min. Core #5 was injected with a lower nanofluid concentration than Core #2, and the tendency is therefore more difficult to observe.

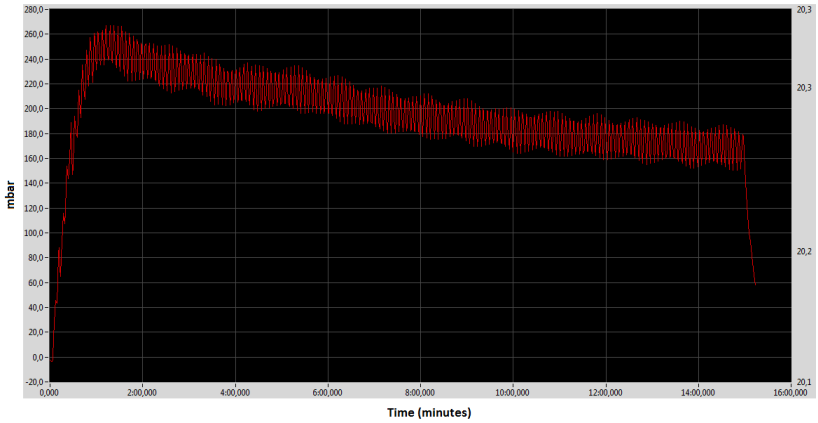

Figure 6.11: Differential Pressure Core #2 - Differential pressure readings for Core #2 after nanoflooding.

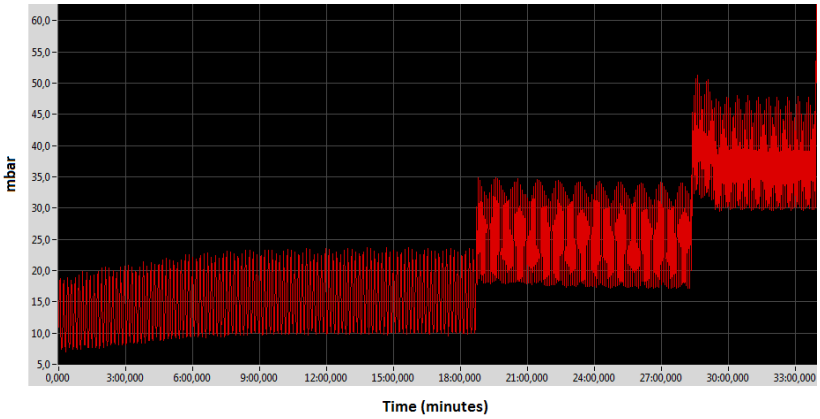

Figure 6.12: Differential Pressure Core #5 - Differential pressure readings for Core #5 after nanoflooding.

6.6 SEM-analysis

The SEM analysis was performed at the Department of Materials Science and Engineering. By taking pictures with a magnitude larger than 30.000 times, observation of nanoparticles on rock surface would be possible. This makes it achievable to substantiate the observed reduction in permeability that took place during flooding with nanoparticles. Initially, Aerosil300 nanopowder was placed on a clean surface and positioned inside the SEM-apparatus. Pictures of SEM-apparatus can be seen in Appendix B.3. Since Aerosli300 nanoparticles have an average size of 7 nm, one nanoparticle would be almost impossible to spot using this device. But nanoparticles have a tendency to cluster together if not solved in a solution, and these could be observed. Figures 6.13 and 6.14 show that nanoparticles form clusters with a size up to 200 nm.

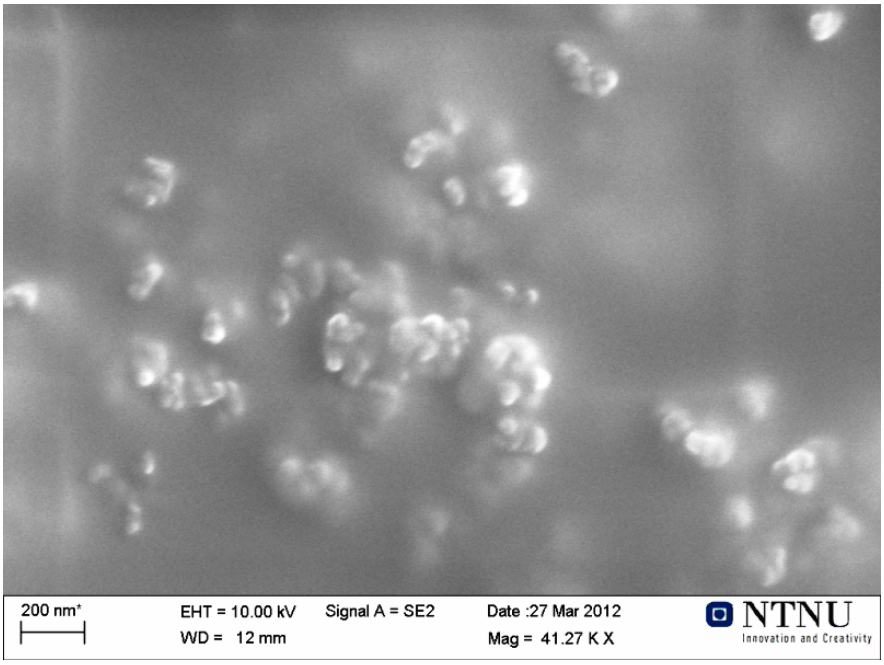

Figure 6.13: NanoPowder - SEM picture of Aerosil300 nanoparticles on clean surface, magnified by 40.000.

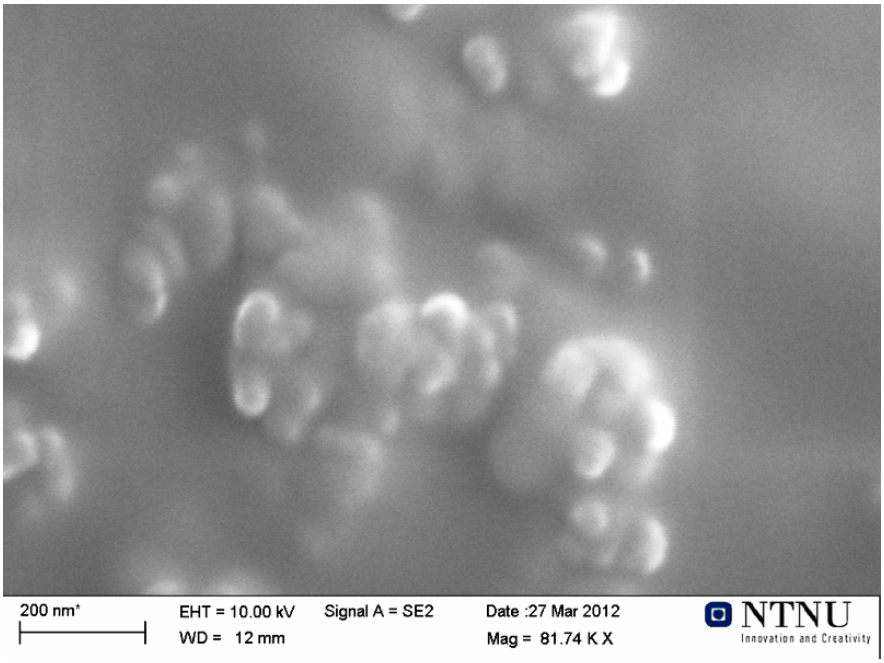

Figure 6.14: NanoPowder - SEM picture of Aerosil300 nanoparticles on clean surface, magnified by 80.000.

Further, core samples where flooding with nanofluid had been performed were to be examined. The samples were crushed, since crushing will leave a clean and pristine surface compared to cutting, and any particle retention could be observed. A core sample was placed inside the SEM-apparatus, Figure B.6, after being coated with a thin carbon layer to assure conductivity.

Core #2 had been flooded with a high concentration of nanofluid, and a large increase in differential pressure had been observed during nanoparticle flooding. It was therefore expected that a high amount of nanoparticles could be observed on grain surfaces. As seen in Figure 6.15, large amounts of cluster-like collections of particles are adsorbed onto a grain surface. It is possible that these are nanoparticle clusters, which implies that nanoparticles tend to cluster and retention within a porous media. This support the results obtained in Section 6.5.2. It is also possible to believe that if the amount of nanoparticles becomes too high, blocking could potentially take place.

Core #4 was injected with a lower nanoparticle concentration than Core #2. Based on the fact that a lower concentration resulted in less permeability impairment, less adsorption on rock surfaces could also be expected. Figure 6.16 shows that the collection of particles is more dispersed for Core#4, and the clusters are significantly smaller. This supports the theory that concentrations play an important role regarding adsorption and retention.

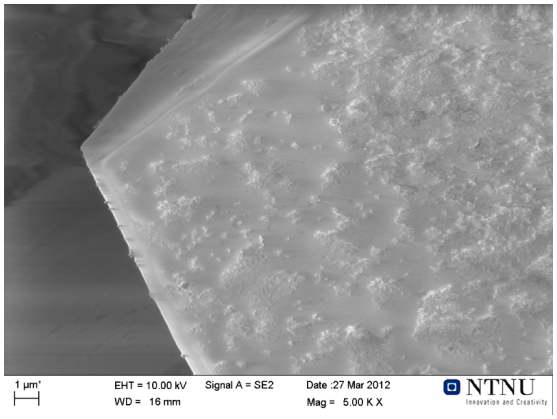

Figure 6.15: Nanoparticles on rock surface after flooding of Core #2.

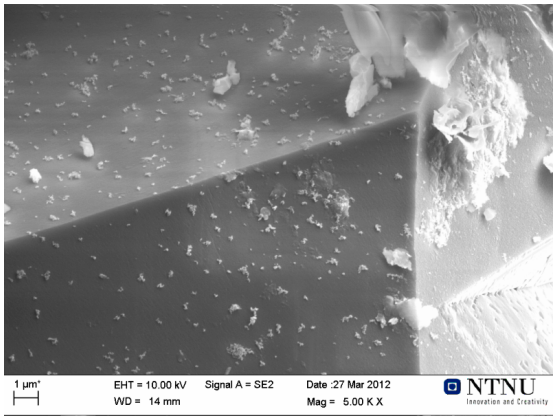

Figure 6.16: Nanoparticles on rock surface after flooding of Core #4.

Examination of the state of nanoparticles before any injection makes recognition of particles on rock surfaces easier. Knowing the form and size of clusters makes it easier to spot and identify remaining particles. It is believed that what is observed on rock surfaces using a scanning electron microscope are remaining particles. The clusters observed on grains look very similar to those observed when examining the nanoparticles in Figure 6.13 and Figure 6.14. Comparison with an untreated core sample also shows that these clusters are not present. Figure 6.17 is taken from a core sample that has not been flooded with nanoparticle solution. On this rock surface, no cluster-like objects are recognizable. Comparing this image with Figure 6.18, taken from a treated sample, a lot of these objects can be observed. It is therefore very likely that particle adsorption onto rock surfaces inside a core sample are recognizable using a SEM-apparatus.

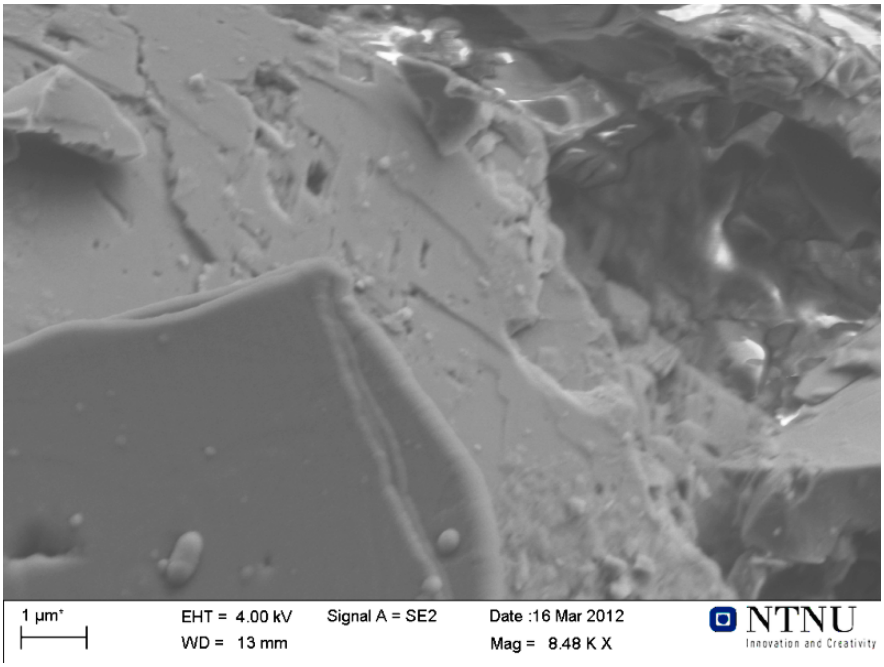

Figure 6.17: SEM-picture - Clean core surface - Clean core surface with no injected nanoparticles.

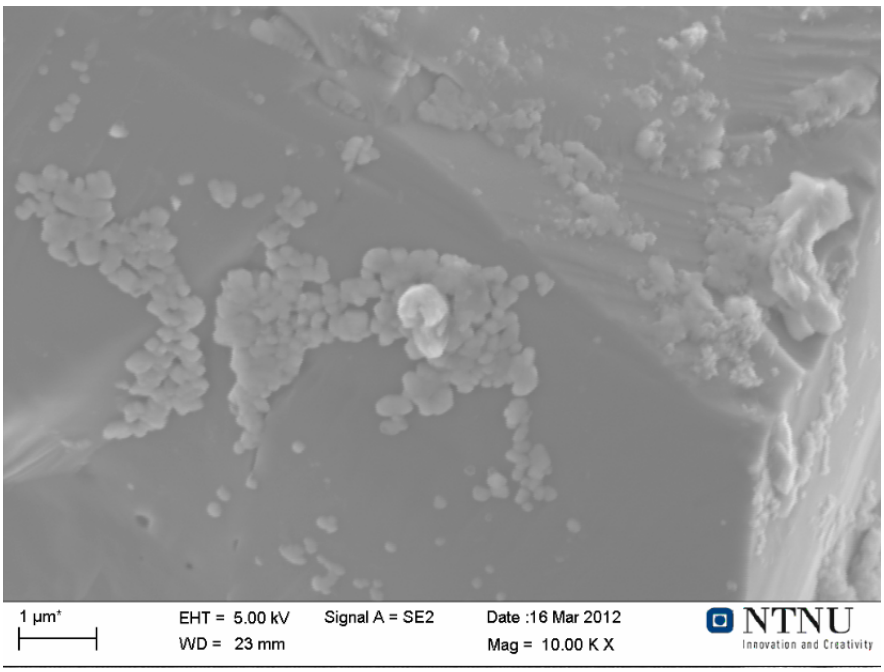

Figure 6.18: SEM-picture - Recognizable nanoparticle clusters - Recognizable nanoparticle clusters on rock surface.

6.7 Establishing Irreducible Water Saturation

Establishment of irreducible water saturation was performed by flooding. Since two flooding scenarios were to be performed, where one of the scenarios required re-saturation of core samples, three cores had to re-establish initial water saturation. This could lead to an unequal distribution of water inside the core sample for the two different establishments. As seen in Figure 6.19, Core #14 and Core #15 have much higher S_{wi} for the second establishment, compared to the first.

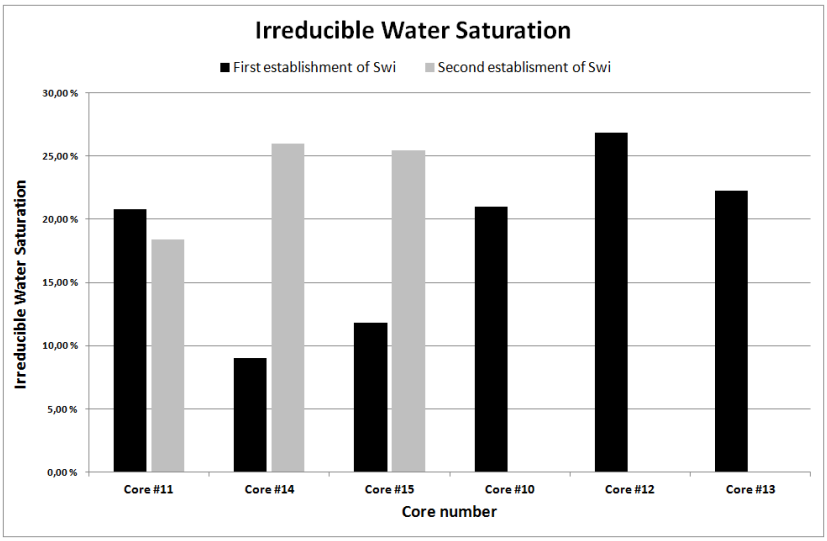

Figure 6.19: Irreducible Water Saturation - Establishment of primary and secondary S_{wi} by sequential waterflooding.

Large disparities from one sequential water flooding to another for the same core sample may indicate that the initial water saturation distribution is not uniform. However, *Viksund et al.* performed experiments on final recovery on Berea sandstone, as percent of original oil in place. The results showed only a minor variation in recovery with change in initial water saturation(60). It is therefore reasonable to expect the final recovery to approximately reach the same percentage, assumed that flooding with brine was performed to displace oil. Still, large disparities in initial water saturation must be taken into account when the results are evaluated. All irreducible water saturations can be seen in Table A.8 in Appendix A.6.

6.8 Flooding

Two scenarios were studied for flooding with nanoparticle solution for EOR purposes. Based on experiments performed on permeability impairment, a nanofluid concentration of 0,01 wt% was decided on. A constant rate for both brine and nanofluid flooding of 0,5 ml/min was applied. Scenario I implemented nanofluid as a tertiary recovery method. In this scenario, brine reduced oil to residual saturation. Continued, approximately two pore volumes of nanofluid were injected in anticipation of improving oil recovery. The second scenario, Scenario II, used nanofluid as a secondary recovery method. Here, two floods were performed for each core. Initially, a first flooding was executed using brine to displace oil. After cleaning, re-saturation and re-establishment of S_{wi}, nanofluid was applied using same procedure to produce oil.

6.8.1 Scenario I

Three core samples were tested using nanofluid as tertiary recovery method. Core #10, #12 and #13 were chosen for this scenario based on liquid permeability measurements.

6.8.1.1 Flooding Core #10

Core #10 was established with an irreducible water saturation of 21 %. Injection of brine was initiated, and only oil production took place until water breakthrough, after approximately 0,35 PV of production. Brine flooding was continued until no more oil production was observed. At this point, the residual oil saturation was 36,61 %, and a recovery factor of 53,68 % was achieved. A total of two pore volumes of brine had been injected. Figure 6.20 shows recovery factor vs. pore volume produced, and is based on numbers from Table A.9 in Appendix A.7.1.

The next step was to continue injection with nanoparticle solution, anticipating improved recovery. Continuing with the same rate as for brine flooding, over two PV of nanofluid was injected. After injecting around one pore volume of this solution, some oil production was observed. This gave, as seen in Figure 6.20, a slight increase in recovery. The recovery factor was improved by 1,58 % and the residual oil saturation after nano flooding was reduced by 1,25 %, to 35,36 %.

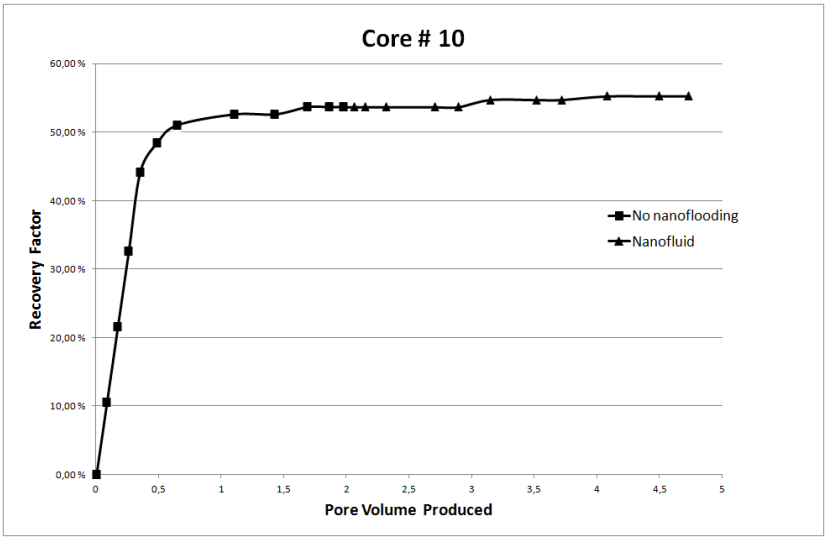

Figure 6.20: Recovery Factor vs. PV Produced Core #10 - Recovery factor vs. pore volume produced for Core #10. Displacing oil to S_{or} by brine before flooding with nanofluid.

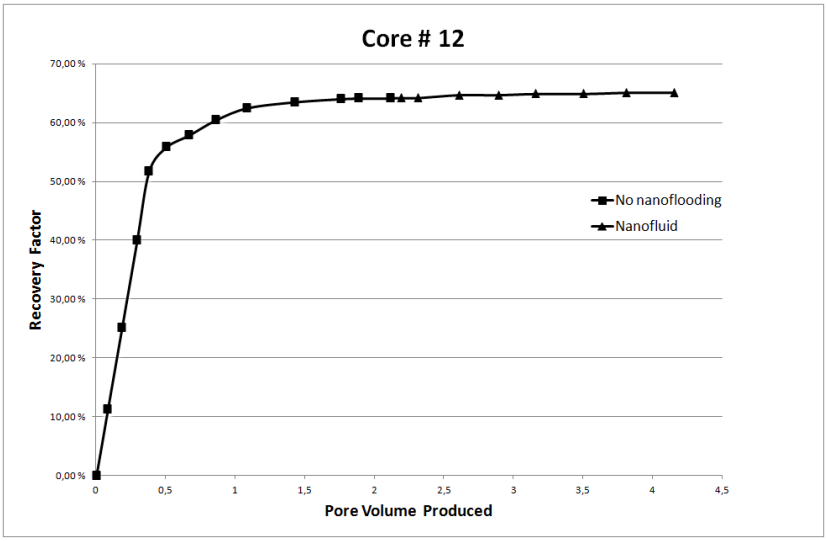

Figure 6.21: Recovery Factor vs. PV Produced Core #12 - Recovery factor vs. pore volume produced for Core #12. Displacing oil to S_{or} by brine before flooding with nanofluid.

6.8.1.2 Flooding Core #12

Core #12 was established with an irreducible water saturation of 26,86 %. Injection of brine was initiated until no more oil was produced. Water breakthrough took place after production of around 0,4 PV. When no more oil production was observed, flooding with nanoparticle solution was conducted. At this point, a recovery factor of 64,21 % and a residual oil saturation of 26,18 % was obtained. A total production of 2,1 PV simultaneously with brine injection was recorded.

Nanofluid flooding was performed under identical conditions. Some oil production was observed, but nanoparticle flooding did not mobilize large quantities of oil. Figure 6.21 shows recovery factor vs. pore volume produced for brine and nanofluid flooding. A small increase in recovery factor, 0,92 %, was recorded. This resulted in an end point residual oil saturation of 25,51 %. Results can be seen in Table A.12 in Appendix A.7.3.

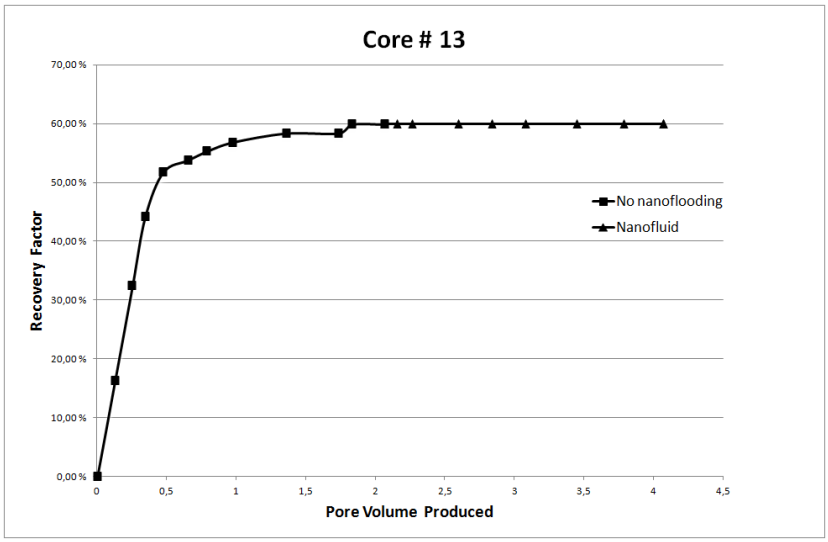

Figure 6.22: Recovery Factor vs. PV Produced Core #13 - Recovery factor vs. pore volume produced for Core #13. Displacing oil to S_{or} by brine before flooding with nanofluid.

6.8.1.3 Flooding Core #13

Core #13 was established with an irreducible water saturation of 22,26 %. Injection of brine was conducted until residual oil saturation was reached. Water breakthrough was observed after producing 0,35 PV of oil. The total recovery factor for brine flooding ended at 59,9 %. This gave a residual oil saturation of 31,18 %. A total production of 2,1 PV was recorded.
Further, nanofluid was injected as a tertiary recovery method, similar to the previous experiments. For this core flood, no oil was mobilized by applying the nanoparticle solution. Figure 6.22 shows recovery factor vs. pore volume produced. As no more oil was produced in terms of using nanofluid, the recovery factor and residual oil saturation were in the end respectively 59,9 % and 31,18 %. Results can be seen in Table A.13 in Appendix A.7.4.

6.8.2 Scenario II

In the second scenario, brine was primarily used to produce all mobile oil. Irreducible water saturation was established for each core, and brine flooding was initiated to obtain residual oil saturation. Core #11, #14 and #15 were chosen for this scenario based on liquid permeability measurements. Secondly, new irreducible water saturation was established for the three core samples after cleaning, and residual oil saturation was reached by using nanofluid as displacing fluid instead of brine.

6.8.2.1 Flooding Core #11

Core #11 was first established with an irreducible water saturation of 20,8 %. Brine flooding was initiated, and production of water was first observed after producing 0,35 PV of oil. Flooding was continued until no more oil was produced, and a recovery factor of 54,64 % was obtained. This resulted in a residual oil saturation of 35,92 %. A total production of 2,1 PV was recorded.

For the second flooding, an irreducible water saturation of 18,37 % was established. The nanoparticle solution was then injected in the same manner as brine had previously been. Water breakthrough was observed after 0,39 PV of production. The total recovery was finally 58,5 %, which gave a residual oil saturation of 33,9 %. Figure 6.23 shows recovery factor vs. pore volume produced for both floods. As observed, they follow the same trend until around 0,5 PV of production. At this point, oil production with brine as displacing fluid levels off. Finally, a difference in approximately 4 % in recovery factor is obtained in favor of nanofluid as displacing fluid. Results can be seen in Table A.10 and Table A.11 in Appendix A.7.2.

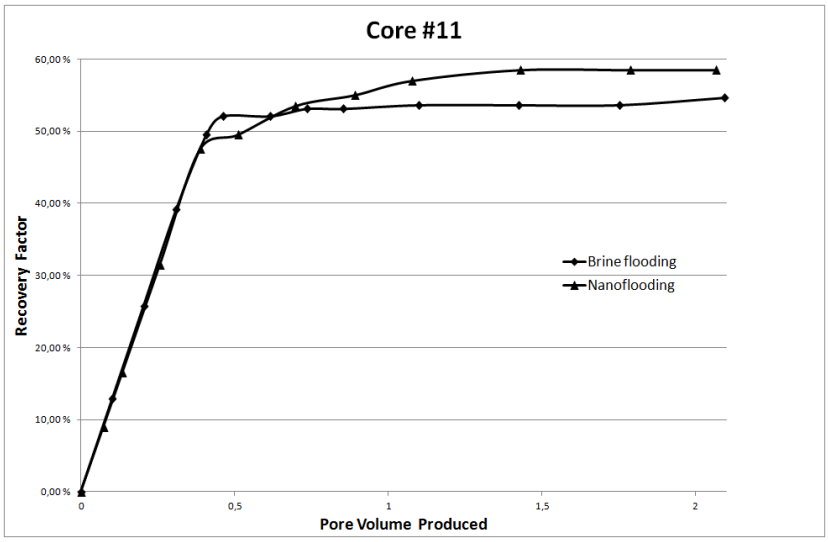

Figure 6.23: Recovery Factor vs. PV Produced Core #11 - Recovery factor vs. pore volume produced for Core #11.

6.8.2.2 Flooding Core #14

Core #14 was initially established with a water saturation of 9 %. Brine flooding resulted in a recovery factor equal to 63 %. A total of 2 PV of oil and water was produced, and a residual oil saturation of 33,7 % was reached.

Secondly, the core was flooded by nanofluid after re-establishment of S_{wi}. The second establishment of irreducible water saturation turned out to be much higher than the first. The second establishment gave an irreducible water saturation of 26 %. Flooding with nanoparticle solution was then commenced, and 2 PV of nanofluid was injected. This resulted in a total production of 62,63 % of original oil in place. A residual oil saturation of 27,7 % was obtained, which was a reduction by 6 % compared to brine flooding. As seen in Figure 6.24, the total recovery factor for both cases ends up at approximately 63 %. However, the reduction in S_{or} is significant. The results can be seen in Table A.14 and Table A.15 in Appendix A.7.5.

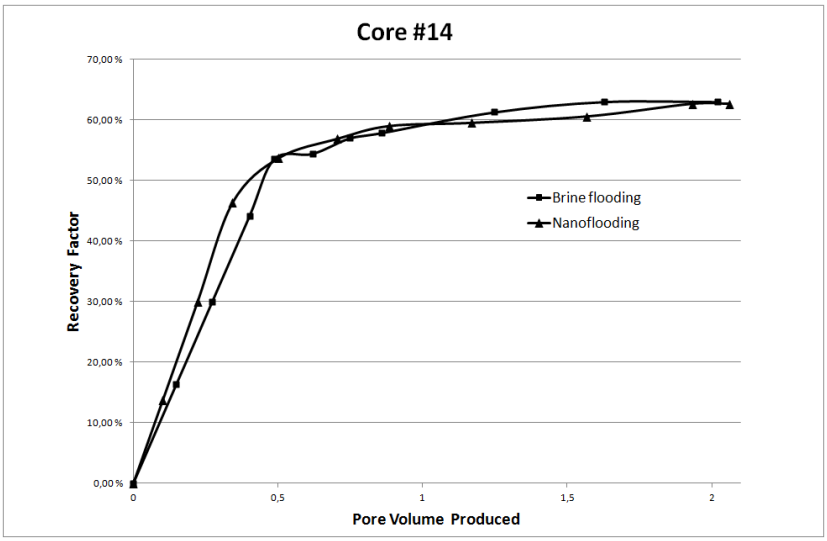

Figure 6.24: Recovery Factor vs. PV Produced Core #14 - Recovery factor vs. pore volume produced for Core #14.

6.8.2.3 Flooding Core #15

Core #15 had an initial water saturation of 11,8 %. Brine flooding was conducted, and a recovery factor of 45,9 % was obtained. This gave a residual oil saturation equal to 47,7 %.

Further, nanofluid was to be injected after cleaning the core, and re-establishing S_{wi}. Equivalent to the results obtained for Core #14, the second re-establishment gave much higher water saturation. After displacing water by oil, 25,4 % water still remained in the core. The differences in primary and secondary re-establishment of S_{wi} will make comparison of results for Core #14 and Core #15 less credible.

Next, nanofluid injection was conducted from the start, until no more oil was produced. A recovery factor of 53,7 % was obtained, and there had been a reduction in residual oil saturation by more than 10 % compared to brine flooding. The residual oil saturation had been decreased from 47,7 % to 34,5 %. Figure 6.25 shows recovery factor vs. pore volume produced when both brine and nanofluid were applied as displacing fluids. The results can be seen in Table A.16 and Table A.17 in Appendix A.7.6.

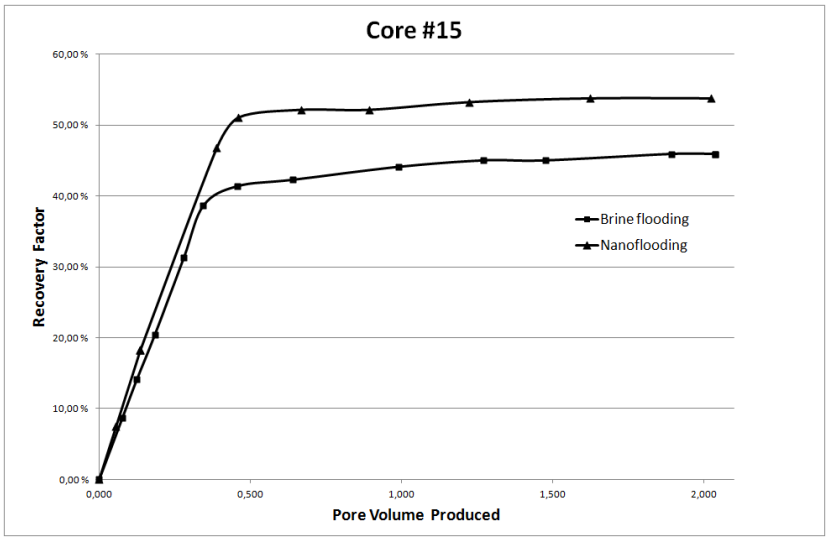

Figure 6.25: Recovery Factor vs. PV Produced Core #15 - Recovery factor vs. pore volume produced for Core #15.

7

Discussion

7.1 Literature Review

There is no doubt that nanotechnology has properties exceeding conventional technology. The high surface area to volume ratio for particles at nanometer scale enhances thermal, chemical and mechanical properties. Applying nanotechnology in oil and gas E&P is considered as one of the most important factors for future development and operations. These particles can improve exploration, drilling operations, construction of platforms, tools and drilling equipment, in addition to being a pioneer in enhanced oil recovery. Many challenges applying nanoparticles in different areas of oil and gas E&P are present, especially concerning EOR purposes. Sufficient laboratory experiments must be performed before applying nanotechnology in large field scale. Knowledge of how nanoparticles affect reservoir properties, how they propagate through a porous media, and how they affect oil mobilization is necessary. However, many of the nanoparticles examined are already present in the reservoir, and of natural character; this makes implementation more acceptable when environmental issues are considered.

7.2 Results

Nanoparticles exhibit interesting properties, but stability over long time periods is difficult to obtain, especially for high concentrations. Smaller particles showed to be more stable in a 1 wt% solution than larger particles, which resulted in the Aerosil300 nanoparticles being chosen for all performed experiments. The stability of nanoparticle dispersions in brine could be a challenge, but applying an ultrasonic reactor solves

this problem at laboratory scale. Nanoparticle solutions have increasing viscosity with increasing concentrations, as well as decreasing pH-value. Increasing viscosities can improve displacement efficiency, but it was believed that applicable concentrations would be too low to increase the viscosity sufficiently. The core samples applied for all flooding experiments have porosity and permeability values ranging for typical sandstone, and are thought to be good reservoir rocks.

7.2.1 Permeability Reduction

Experiments performed on permeability reduction applying nanoparticle solutions gave results that in many ways were expected. A variety of concentrations, injection volumes and rates were tested to determine the effect of nanofluid flooding through core samples. All measurements gave negative results, in the sense that the permeability was reduced. There are several possible phenomena when injecting particles through a porous media; adsorption, desorption, blocking and transportation. Both adsorption onto rock surfaces and blocking of pore throats are thoroughly presented in Chapter 4. When permeability reduction is observed, it can be explained by one of these incidents. Figure 6.6 in Section 6.5.2 shows how differential pressure increases when injecting a nanoparticle solution. This is a clear indication that particles are decreasing the ability of water to flow through a porous medium. Hydrophilic silica nanoparticles which are applied in this thesis should render a water-wet rock even more water-wet. As presented by *Ju and Fan*, if the total surfaces per unit bulk volume of the porous media are completely covered by polysilicon nanoparticles adsorbed on pore body surfaces, permeability will be affected by the wetting properties of PN. If a water-wet rock becomes more water-wet, a higher percentage of water will become immobile. This will again result in less space for free water to be transported and a higher ΔP is required to obtain the same rate, which will result in permeability reduction. However, the Berea sandstone applied in these experiments is already virtually completely water-wet, and this effect would therefore be minimal. It is therefore likely that the phenomenon of pore blockage, as mechanical entrapment and log-jamming, affects the permeability to a greater extent than surface coating. The Aerosil 300 nanoparticles applied in these experiments have an average particle size of 7 nm. Based on the fact that filtration through a 25 nm filter only had a minor effect on the magnitude of reduction, in addition to pore throats sizes being several times greater than 25 nm, mechanical entrapment is probably not an issue.

Changing the concentration proved, however, to have a gradually increasing effect on the impairment. A higher concentration gave a higher permeability reduction. For high concentrations the impairment can be explained by adsorption, accumulation and blocking of pore spaces. For low concentrations, with low injection volumes, it is possible that a thicker water film caused by adsorption of hydrophilic NP affects the permeability impairment to the same degree as blocking. For high concentrations, a reduction in the range of 90 % was observed. A reduction in this range would not be accepted for application in any oil reservoir. The results obtained show that that a higher concentration than 0,1 wt% would most likely not be applicable.

The rate plays an important role when injecting and producing fluids from an oil reservoir. For this study, too few experiments were performed on the effect of varying rate. Only two comparisons applying different rates were investigated. This is not a sufficient amount of comparisons to make a conclusion on how rate affects the permeability impairment as a cause of nanofluid flooding. The experiments conducted showed however a lower impairment for lower rate. According to *Ju and Fan*, *Gruesbeck and Collins* present a theory of an existing critical velocity. Above this velocity, both retention and entrainment will occur, while only retention will take place below the critical velocity(34). This theory states that a higher velocity will result in higher reduction, since entrainment will take place in addition to retention. When reducing the rate from 0,5 ml/min to 0,1 ml/min, a reduction in impairment was observed. There is though, no clear indication that this is a result of exceeding a critical velocity. Nevertheless, when rate is increased, a higher amount of particles are possible to be entrapped due to log-jamming effect. If a higher rate is kept constant over a long time compared to a lower rate, it is reasonable to believe that the entrainment becomes higher.

It is also important to know the effect of altering pore volume injected. As for varying rate, too few supporting experiments were performed in this case. The results obtained were contradicting, and neither result could be neglected. However, irrespective of the number of test performed, each core sample has different properties, and results will vary as a consequence of this. Therefore, it is reasonable to believe that the

results that show an increase in impairment with increasing volume injected are correct. There have been clear indications throughout all floods performed, that increasing the amount of nanoparticles injected, either volume or concentration, increases the impairment. However, none of the results obtained in the study resulted in appreciation of permeability. This is a clear indication that nanoparticle flooding through a porous media reduces the permeability to an extent highly dependent on varying parameters. It is also reasonable to believe that the permeability reduction will occur with a higher percentage closer to the inlet than the outlet. A numerical solution presented by *Ju and Fan* show the permeability relation (K/K_o) as a function of dimensionless distance, where K_o is initial permeability. The ratio decreases with increasing PV injected, and show a gradual increase towards initial permeability with increasing dimensionless distance(34). This means that for a higher injection volume, the permeability impairment is larger. This numerical solution supports the result obtained for Core #6 and Core #7, which suggest a higher reduction in permeability with increasing volume injected.

There are also possibilities that clay swelling can cause reduction in permeability. Swelling of clay minerals within the rock structure is an important mechanism causing formation damage. The clay content in sandstones is not large, however, it tends to cover the surfaces of pore spaces, and swelling can cause relatively high formation damage. The clay content in the Berea sandstones applied in all flooding experiments consists of illite(61). According to *Abbasi et al.*, the existence of kaolinite or illite clay minerals in sandstone show no important swelling induced impaired permeability(62). Reduction in permeability due to clay swelling did therefore not cause the permeability impairments observed. Nevertheless, other formations consisting of different clay minerals can have formation damage caused by swelling, in addition to the damage caused by nanoparticles. It is reasonable to believe that clay swelling and nanoparticle damage occurring simultaneously will enhance the total damage. Consequently, even though clay swelling does not affect the permeability impairment, consciousness regarding the problem is important.

Another observation that was of interest when performing permeability impairment experiments, was the repetitive reduction in ΔP when injecting brine after nanoparticle flooding. Figure 6.11 shows how ΔP gradually decreases with time when brine is

injected. This suggests that some of the nanoparticles trapped are removed, replaced or rearranged. Most of the trapped nanoparticles have been retained close to the inlet, and the permeability reduction would therefore be larger at the inlet than at the outlet. When injecting brine after nanoparticle flooding, some of the particles which are either settled by gravity, blocking pore throats or adsorbed, will be mobilized and transported closer to the outlet or out of the core. This can result in a lower concentration of nanoparticles inside the core due to deportation, resulting in a lower ΔP. Or, a continuous uniform distribution throughout the core could have been obtained. This deportation caused by continuous brine flooding following nanoparticle flooding results in a small permeability appreciation. The appreciation is not in the same order of magnitude as the impairment, but it indicates that some nanoparticles inside a core sample are mobile after injection.

7.2.2 Establishment of Irreducible Water Saturation

Establishment of irreducible water saturation was as mentioned, performed by flooding. Establishment of S_{wi} by flooding often results in relatively high water saturation, and porous plate method would have been a better option to obtain low saturations. Porous plate is however time-consuming, and flooding was therefore chosen. As presented earlier, large deviations from primary to secondary establishment was obtained. For Core #10, #12 and #13, where nanoparticle flooding was to be implemented as tertiary recovery method, no re-establishment of water saturation was conducted, and variation in S_{wi} was negligible. For Core #11, #14 and #15, two similar floods with following comparison should take place. For two of these core samples, there were large variations in primary and secondary establishment of irreducible water saturation. A higher irreducible water saturation results in more immobile water inside the core. However, *Viksund et al.* addressed that differences in S_{wi} within 0-30 % have virtually no effect on the final recovery factor when applying synthesized oil. The displacement process is independent of the percentage of pore volume initially occupied by water, and the residual oil saturation also prove to be almost independent of S_{wi} up to 30 %, for Berea sandstone(60). It is therefore reasonable to expect small variations in recovery factor for sequential flooding, even though irreducible water saturation is varying. This makes comparison of results possible, but inequalities must be taken into consideration when discussing further results.

7.2.3 Flooding experiments

The two scenarios examined have been presented previously. In advance, it was not expected that injection of hydrophilic silica nanoparticles would mobilize large amounts of additional oil as a tertiary recovery method. This expectation was primarily based on similar experiments presented in the literature, such as *Skauge et al.*, where silica particles showed to propagate easily through a core without mobilizing oil(39).

Three core floods were performed applying nanofluid as a tertiary recovery method. For each case, around 2 PV of a 0,01 wt% nanoparticle solution was injected after reaching residual oil saturation. Only Core #10 and Core #12 had some additional oil recovery, while no extra oil was mobilized for Core #13. Berea Sandstone saturated with synthetic oil tend to approach a completely water-wet state. Even though the total surface area per unit bulk volume is completely covered by particles that are adsorbed, and wettability is determined by these nanoparticle properties, the system will not be supplementary water-wet. Altering the wettability of a Berea Sandstone saturated with synthetic oil by hydrophilic silica nanoparticles is not expected to be the mechanism that enhances any oil production, since surface wetting most likely will remain unchanged. It is therefore reasonable to assess the theory presented by *Skauge et al.* When injecting silica particles through a core sample, smaller and narrower pores will lead to higher velocity. In this case, silica nanoparticles are possible to accumulate, and a log-jamming effect could take place. *Skauge et al.* addresses this possibility for oil mobilization, but they also state that a certain viscosity is required to generate an oil bank, and produce oil(39). An increase in viscosity was by *Skauge et al.* obtained by polymer additives. The experiments performed in this master's thesis did not have any additives in the nanoparticle solution, and the required viscosity is therefore not present. However, log-jamming will cause particles to gradually accumulate and can block pores larger that the particle size. This happens due to the mass differences between particles and solvent. Since the rate is kept constant through the pore system, any blocking of pore throats may enhance the flooding in other areas. An increase in velocity through a pore space may overcome the capillary pressure that traps the oil, and mobilize very small amounts of additional oil.

The second scenario that is likely to mobilize oil droplets after residual oil saturation is obtained, is the effect of disjoining pressure. In a completely water-wet core sample, the residual oil will be trapped on the surface of a water film by capillary forces. To mobilize this oil, these capillary forces must be overcome. In more conventional EOR-methods, surfactant and low salinity flooding are examples of methods to improve oil recovery by reducing interfacial tension or alter the wetting phases respectively. When injecting nanoparticles in solution, these particles can be structured inside a wedge film between a water surface and an oil droplet. The particles will then execute an additional pressure at the head of the wedge, between the oil droplet and water film as seen in Figure 4.3. As presented by *Wasan et al.*, the excess pressure will spread onto the surface between the liquids, and separate the two phases(54). This phenomenon could explain the mobilization of oil that took place during tertiary flooding with nanoparticles. An investigation performed by *Sefiane et al.* concluded that the spreading velocity increases as nanoparticle fraction is increasing within a range of 0-1 %(52). This implies that a higher concentration could cause a higher disjoining pressure, since a larger amount of nanoparticles can structure inside the wedge film and provide the excess pressure. This could probably result in mobilization of larger oil droplets. However, increasing the concentration also results in more severe permeability impairment, as examined earlier. It is not desirable to reduce the permeability to a too great extent. This makes the combination of achievable mobilization of oil as a result of spreading of hydrophilic nanoparticles, and permeability impairment an important topic.

Flooding scenario number two implemented nanoparticle solution as a secondary recovery method. The expectation for applying hydrophilic silica nanoparticle in an early phase was to possibly enhance the displacement efficiency. The results obtained were encouraging, but inequalities in establishment of irreducible water saturation for primary and secondary flooding made comparisons difficult. S_{wi} for Core #11 was however around 20 % for both floods. For this core, an improvement in total recovery of approximately 4 % in favor of nanoparticle solution as displacing fluid was achieved. For Core #14 and Core #15, large disparities in establishment of S_{wi} was observed. However, the results obtained when flooding with nanofluid are remarkable. *Viksund et al.* reported that the residual oil saturation showed to be almost independent of initial water saturation for Berea sandstones(60). This should result in no or relatively

small variations in S_{or} regardless of whether initial water saturation is 10 or 20 %. The results for Core #14 and Core #15 did however show similar, or higher recovery factor when nanoparticle solution was applied as displacing fluid compared to brine flooding. In addition, a decrease in residual oil saturation was evident in all three cases.

There are several possible explanations of the improvement in recovery and reduction in residual oil saturation for the three floods. As experimental results show, the viscosity of a nanoparticle solution increases with increasing concentration. When displacing oil with a fluid with higher viscosity than brine, a better mobility ratio is obtained. This results in a more "piston like" displacement, and less oil will be left behind the water front. The fact that the concentration applied for displacement purposes was 0,01 wt%, the increase in viscosity compared to brine is probably not high enough to improve the displacement efficiency significantly. Applying a higher concentration than 0,01 wt% is possible to enhance the displacement efficiency to some extent, but again, the effect on permeability impairment must be considered. It is, nevertheless, conceivable that nanoparticles somehow can structure as a film at the water front. This structuring could result in an even higher viscosity at the front, and thus a better sweep efficiency than what is obtained by brine flooding. These theories are not widely discussed in the literature, even though they could be possible explanations. Other theories are discussed to a much greater extent, and show to be more plausible.

The mechanisms that are more widely discussed in the literature may explain the increase in recovery factor and the reduction in residual oil saturation. As discussed in the first flooding scenario, nanoparticles can create an excess pressure inside the wedge film between two phases. When nanoparticles are injected as a secondary recovery method from the beginning, the particles may structure inside a wedge film at an earlier stage than when injected as a tertiary recovery method. This may result in mobilization of larger oil droplets than what is being mobilized by brine flooding, and less oil is left behind the front. Oil droplets that are trapped by capillary forces, either on rock surface or on a water film, can be mobilized by this excess pressure between two phases. There can also be other factors that explain the result, which are not affected by injection of nanoparticle solution. When obtaining dissimilar water saturations, a different distribution in the core sample is likely to occur. This can result in different

mobilization for an identical core for sequential flooding. Oil can be trapped in larger pores, and water can more easily displace it. However, the results indicate that nanoparticles are likely to affect the displacement efficiency, even though oil distribution is varying. The causes of improved recovery and reduced S_{or} can be several when using hydrophilic SiO_2 nanoparticles. A more extensive study is therefore required to assure whether the oil is mobilized by alternation of surface wetting, viscosity changes, the effect of an excess pressure between two phases, or that inequalities between sequential floods are dominating.

7.2.4 SEM-analysis

SEM- and TEM-apparatus have been used in many studies to detect nanoparticle retention on rock surfaces in porous media. Knowledge of adsorption and entrainment are important to be able to understand how nanoparticles propagate through a reservoir. Nonetheless, there are some challenges regarding picturing of rock samples using a SEM-apparatus. Berea Sandstone is not highly conductive, and the reflections of electrons depended on how the surface of the medium was oriented relative to the electron source. Coating the samples with a thin carbon layer, in addition to covering all sides except the one to be examined with aluminum foil, enhanced the conductivity. This resulted in higher reflection frequency of electrons, and relatively good pictures were obtained. *Kanj et al.* presented work done to identify usable size of nanoparticles. In their report, ESEM-pictures show rock surfaces coated with nanoparticles(38). A comparison with photos obtained from SEM-analysis as presented in Section 6.6, clearly indicates similarities in the observations. This comparison supports the idea of nanoparticle adsorption on rock surfaces. Since access to the nano-laboratory was necessary to examine the effluent by nanosight, SEM-analysis was the only visible indication of nanoparticle retention. This observation supports the theory of nanoparticle solution affecting the permeability when propagating through a porous media. The pictures obtained show that a higher concentration results in a larger adsorption on grain surfaces. Comparing the observations from SEM-analysis and the results obtained from permeability impairment experiments, show that they are unambiguous. Particle retention is proven to be existent, and both experiments indicate that a higher nanoparticle concentration result in higher entrainment.

7.3 Experimental Procedure and Error Margins

Performing laboratory experiments are time-consuming and precise work. The results are depending on numerous parameters, and small errors can end up in relatively large deviations in the end. Therefore, evaluation and understanding of results are important. Throughout this thesis, several deviations were observed. Deviations and error margins will always occur, and are impossible to avoid. All manual readings will have larger deviations than automatic readings, since they are more inaccurate. An error margin of 1 % for porosity readings can after calculations results in a deviation in porosity by 2,5 %. As an example, when performing flooding experiments for EOR purpose, irreducible water saturation, residual oil saturation and recovery factor are all a function of porosity. If porosity has an error margin of 1 %, this will result in differences for S_{wi}, S_{or} and RF varying from 1-2 %. This shows how important it is to be aware of deviations from readings, and especially manual readings.

Another deviation that clearly took place during the experimental procedure was the pump efficiency. When applying cylinders for different fluids, there were some clear indications that the pump was not able to deliver a constant rate throughout the floods. This could possibly result in differences regarding the displacement efficiency, which again could result in variation in oil mobilization from case to case. In addition, a pressure gauge was not applied when performing flooding for EOR purpose. A limited amount of pressure gauges are available at the laboratory, and it was therefore not accessible. This made it impossible to observe pressure variations when flooding with nanoparticles for EOR purpose. However, based on the result obtained throughout the permeability impairment experiments, it was believed that the pressure would increase within the same range. Variations in oil mobilization can in worst case be caused by pump effect and other error margins. It is believed that the work performed is accurate, and that the results are not affected by deviations to a too great extent. However, too few experiments are performed for the different cases. This makes it impossible to make definite conclusions. The results are generally pointing in the same direction, indicating that several experiments will support the already achieved results.

7.4 Summary

Overall, it is clear that silica nanoparticles affect reservoir properties. There is no doubt that permeability impairment takes place, and that it is highly dependent on particle size, concentration, rate and PV injected. However, applying hydrophilic silica nanoparticle for enhanced oil recovery in a water-wet Berea Sandstone did not mobilize appreciable additional amount of oil. Applying nanoparticle solution as a tertiary recovery method, mobilized insufficient amounts of oil. As secondary recovery method, the nanoparticle solution reduced the residual oil saturation in all three cases, even though higher irreducible water saturation was present initially. There is no clear answer for the cases where additional oil is mobilized, but, the theory of disjoining pressure is supported. Since the particles most likely do not mobilize oil by altering the wetting phase, their size and ability to be transported through a porous media indicates that this is the most plausible theory. Applying small particles and injecting with low concentration will cause a less severe damage of reservoir properties. Small particles are also more likely to structure inside a wedge film between to liquids. Applying as small nanoparticles as possible could therefore result in mobilization of smaller oil droplets, and reduce the residual oil saturations even more, without resulting in too high permeability impairment.

Regardless of the experiments performed on oil mobilization, the SEM-analysis show that particles adhere and spread on rock surfaces. This is a clear indication that the wetting phases can be changed due to particle adsorption. Improving oil recovery by adding hydrophilic particles in a mixed-wet core sample is therefore plausible. If aging of core samples had been performed, and a crude oil had been applied, an intermediate wetness would have been obtained. Applying hydrophilic particles in a mixed-wet core sample may alter the wettability to a water-wet state. Water-wet core samples produce almost all mobile oil before water breakthrough. In an oil-wet or mixed-wet system, water breakthrough occur much earlier, and most of the oil is recovered during a long period where oil and water is produced simultaneously(63). If the surface wetting of a reservoir could have been changed from oil-wet to water-wet early in the production phase, this could have been of great economic interest. Time value of money states that money today is more worth than the same amount of money later. Companies

therefore want to earn their money as close to this date as possible, and hydrophilic nanoparticle addition in an oil- or mixed-wet system can accelerate the production by changing the systems wetting phase.

The experiments performed in this thesis have only addressed the effect of implementing hydrophilic silica nanoparticles in Berea Sandstone. The experiments performed show acceptable permeability impairments for relatively low concentrations, and interesting results when applying SiO_2 nanoparticles for oil mobilization purposes. It is necessary to execute more experiments that support the already achieved results. With an adequate number of measurements, one can to a greater extent be able to conclude about the causes of impariment with greater certainty. This will give a better understanding of the effect of hydrophilic nanoparticles in reservoir systems.

8

Conclusion

Nanotechnology in the petroleum industry has gained enormous interest the recent years, which is reflected in the amount of literature available. Nanoparticles for EOR purposes seem gradually to become the cutting-edge technology.

Hydrophilic silica nanoparticles have through experimental work showed to propagate through a porous media. The particles caused permeability impairment, which was highly dependent on varying parameters, especially concentration. Both permeability reduction experiments and SEM-analysis showed similar results, where both indicated entrainment and adsorption onto rock surfaces. Large concentrations yielded too high impairment, and a nanoparticle concentrations should not exceed 0,1 wt %.

The silica nanoparticles had various effects on enhancing oil recovery. The nanoparticle solution utilized did not mobilize sufficient oil when applied as a tertiary recovery method; where it only increased recovery with 0-1 % above secondary baseline. Interesting results were however obtained when nanoparticle solution was used as a secondary recovery method. Here, a significant decrease in residual oil saturation varying from 2-13 % was observed for the three floods, and an increase in recovery factor varying from 0-8 % was obtained. The potential for hydrophilic silica nanoparticles as an EOR-agent is existing, but it is clear that a water-wet reservoirs are not the best target area. Applying hydrophilic silica nanoparticles in a different wetting system will possibly show a much more promising result.

9

Recommendation

This master's thesis is the first thesis carried out at the Department of Petroleum Engineering and Applied Geophysics at NTNU, applying nanoparticles for EOR purposes. There was little experience in the field in advance, which made a lot of trial and error was inevitable. It is much easier in hindsight to see what should have been done differently, and where one should have been more consistent. Based on the experience obtained throughout this thesis, some recommendations for further work will be presented.

A closer study of how hydrophilic silica nanoparticles alter the wettability of a rock surface should be executed. This would give a better understanding on how it should be implemented for EOR purposes. Several flooding experiments examining the effect of permeability impairment should be conducted. The results obtained in this thesis show distinct results regarding reduction in permeability, but multiple results are needed in order to be able to conclude about the causes of impairment with greater certainty.

Establishment of S_{wi} should for further experiments be performed using the porous plate method. In comparison, identical S_{wi} for sequential flooding are desirable. A lower and more consistent S_{wi} is more easily obtained by porous plate method. Finally, aging of core samples using crude oil would be of great interest. As discussed earlier, obtaining a mixed-wet system will make it possible to examine the effect of wettability alternation when flooding with hydrophilic nanoparticles. This could enhance the recovery, and be of economical advantage as the oil could be produced more rapidly.

References

[1] "U.S. Environmental Protection Agency `http://www.energystar.gov/index.cfm?c=business.bus_energy_strategy`," Entered 07.02.2012. iii

[2] X. Kong and M. M. Ohadi 2010, "**Application of Micro and Nano Technologies in the Oil and Gas Industry- An Overview of the Recent Progress**," *Abu Dhabi International Petroleum Exhibition & Conference*, 1-4 November 2010. iii, vii, 16, 18

[3] Bob Tippee 2009, "**Nanotechnology Seen Boosting Recovery Factor**," *Oil and Gas Journal*, 9. April 2009. iii

[4] I. N. Evdokimov, N. Y. Eliseec, A. P. Losev, and M. A. Novikov 2006, "**Emerging Petroleum-Oriented Nanotechnologies for Reservoir Engineering**," *SPE Russian Oil and Gas Technical Conference and Exhibition*, 3-6 October 2006. iii

[5] B. Ju, D. Shugao, L. Zhian, Z. Tiangoa, S. Xiatao, and Q. Xiaofeng 2002, "**A Study of Wettability and Permeability Change Caused by Adsorption of Nanometer Structured Polysilicon on the Surface of Porous Media**," *SPE Asia Pacific Oil and Gas Conference and Exhibition, Melbourne, Australia*, 8-10 October 2002. 1, 23, 24

[6] B. Engeset 2011, "**Project Thesis - The Use of Nanotechnology in the Petroleum Industry**," December 2011. 1, 7, 14, 15

[7] "Nanowerk `www.nanowerk.com/nanotechnology/introduction/introduction_to_nanotechnology_1a.php`," Entered 10.02.12. 1, 2, 3

[8] R. Kelsall, I. Hamley, and M. Geoghegan, "**Nanoscale Science and Technology**," *John Wiley & Sons Ltd*, 2005. 1, 2, 3, 4

[9] M. Kohler and W. Fritzsche, "**Nanotechnology - An Introduction to Nanostructuring Techniques** Second Completly Revised Edition," *WILEY-VCH Verlag GmbH & Co. KGaA*, 2007. 2, 4

[10] Richard Freyman 1960, "**There's Plenty of Room at the Bottom**," *Engineering and Science*, 1960. 3

[11] J. F. Mongillo, "**Nanotechnology 101**," *Greenwood Press*, 2007. 3, 4

[12] M. Abtahi and O. Torsæter, "**Experimental Reservoir Engineering - Laboratory Workbook**," 6, 7, 8, 9, 10, 11, 12, 28, 30, 32

[13] Oilfield Glossary - Permeability, "`http://www.glossary.oilfield.slb.com/Display.cfm?Term=permeability`," Entered 25.02.2012. 6

[14] Oilfield Glossary - Wettability, "`http://www.glossary.oilfield.slb.com/Display.cfm?Term=wettability`," Entered 25.02.2012. 8

[15] O. Torsæter, "**Lecture Notes - Unconvential Reservoir**," *Fluid Properties Part 1 & 2*, 2010. 11, 12

[16] Engineering Toolbox, "**Fluid Density Temperature Pressure** - `http://www.engineeringtoolbox.com/fluid-density-temperature-pressure-d_309.html`," Entered 09.04.2012. 12

[17] S. Kakac and A. Pramuanjaroenkij 2009, "**Review of Convective Heat Transfer Enhancement with Nanofluids**," *International Journal of Heat and Mass Transfer*, 26 March 2009. 14

[18] M. Alaskar, M. Ames, S. Connor, C. Liu, Y. Cui, K. Li, and R. Horne 2011, "**Nanoparticle and Microparticle Flow in Porous and Fractured Media: An Experimental Study**," *SPE Annual Technical Conference and Exhibition held in Denver, Colorado, USA*, 30 October - 2 November 2011. 14

[19] P. Kearey, M. Brooks, and I. Hill, "**An Introduction to Geophysical Expolration**," *Blackwell Science Ltd.*, 2002. 14

[20] S. Al-Mahrooqu and W. Walton 2011, "**Well Logging and Formation Evaluation Challenges in the Deepest Well in the Sultanate of Oman (HPHT Tight Sand Reservoirs)**," *SPE Middle East Unconventional Gas Conference and Exhibition*, 31 January-2 February 2011. 14

[21] Advanced Energy Consortium 2008, "**Request for Proposal Micro- and Nanosensors for Oil and Gas Exploration and Production Applications**," Issued 14 July 2008. 14

[22] R. Krishnamoortu 2006, "**Extracting the Benefits of Nanotechnology For the Oil Industry**," *JPT, Society of Petroleum Engineers*, November 2006. 15, 16

[23] A. Shihab-Eldin 2002, "**New Energy Technologies: Trends in the Development of Clean and Efficient Energy Technologies**," *Organization of the Petroleum Exporting Countries - OPEC Review*, December 2002. 15

[24] M. Amanullah and A. M. Al-Tahini 2009, "**Nano Technology - Its Significance in Smart Fluid Development for Oil and Gas Field Application**," *SPE Saudi Arabia Section Technical Symposium, AlKhobar, Saudi Arabia*, 9-11 May 2009. 15

[25] M. Amanullah, M. Al-Arfaj, and Z. Al-Abdullatif 2011, "**Preliminary Test Results of Nano-based Drilling Fluid for Oil and Gas Field Application**," *SPE/IADC Drilling Conference and Exhibition, Amsterdam, The Netherlands*, 1-3 March 2011. 15

[26] P. Pourafshary, S. Azimipour, P. Motamedi, M. Samet, S. Taheri, H. Bargozin, and S. Hendi 2009, "**Prior Assessment of Investment in Development of Nanotechnology in Upstream Petroleum Industry**," *SPE Saudi Arabia Section Technical Symposium, AlKhobar, Saudi Arabia*, 9-11 May 2009. 16

[27] T. Huang and J. B. Crews 2007, "**Nanotechnology Applications in Viscoelastic Surfactant Stimulation Fluids**," *European Formation Damage Conference, Scheveningen, The Netherlands*, 30 May-1 June 2007. 16

[28] N. Nassar, M. Al-Jabari, and M. Husein 2008, "**Removal of Asphaltenes from Heavy Oil by Nickel Nano and Micro Particle Adsorbents**," *Proceeding (615) Nanotechnology and Applications*, January 1 2008. 16

[29] L. Zang, J. Yyan, H. Liang, and K. Le 2008, "**Energy From Abandoned Oil and Gas Reserves**," *SPE Asia Pacific Oil and Gas Conference and Exhibition, Perth, Australia*, 20-22 October 2008. 16

[30] R. D. Shah 2009, "**Application of Nanoparticle Saturated Injectant Gases for EOR of Heavy Oil**," *SPE Annual Technical Conference and Exhibition, New Orleans, Louisiana, USA*, 4-7 October 2009. 17

[31] N. Le, D. K. Pham, K. H. Le, and P. T. Nguyen 2011, "**Design and Screening of Synergistic Blends of SiO_2 Nanoparticles and Surfactants for Enhanced Oil Recovery in High-Temperature Reservoirs**," *Advances in Natural Sciences: Nanoscience and Nanotechnology 2*, Published 21 July 2011. 17

[32] B. Suleimanov, F. Ismalov, and E. Veliyev 2011, "**Nanofluid for Enhanced Oil Recovery**," *Journal of Petroleum Science and Engineering*, 6 June 2011. 17

[33] M. O. Onyekonwu and N. A. Ogolo 2010, "**Investigating the Use of Nanoparticles in Enhancing Oil Recovery**," *Nigeria Annual International Conference and Exhibition, Tinapa - Calabar, Nigeria*, 31 July - 7 August 2010. 17, 25

[34] B. Ju and T. Fan 2008, "**Experimental Study and Mathematical Model of Nanoparticle Transport in Porous Media**," *Powder Technology*, Accepted 22 December 2008. 17, 25, 65, 66

[35] T. Zhang, A. Davidson, S. L. Brytant, and C. Huh 2010, "**Nanoparticle-Stabilized Emulsions for Application in Enhanced Oil Recovery**," *SPE Improved Oil Recovery Symposium, Tulsa, Oklahoma, USA*, 24-28 April 2010. 18

[36] J. Dickson, K. Johnston, and B. Binks 2004, "**Stabilization of Carbon Dioxide-in Water Emulsions with Silica Nanoparticles**," *Langmuir The Acs Journal Of Surfaces And Colloids*, August 14 2004. 18

[37] S. S. Adkins, D. Gohil, J. L. Dickson, S. E. Webber, and K. P. Johnston 2007, "**Water-in-Carbon Dioxide Emulsion Stabilized by Hydrophobic Silica Particles**," *Physical Chemistry Chemical Physics Issue 48*, November 8 2007. 18

[38] M. Y. Kanj, Z. AlYousif, and J. Funk 2009, "**Nanofluid Coreflood Experiment in the ARAB-D**," *SPE Saudi Arabia Section Technical Symposium and Exhibition, Aikhobar, Saudi Arabia*, 9-11 May 2009. 18, 71

[39] T. Skauge, K. Spildo, and A. Skauge 2010, "**Nano-sized Particles For EOR**," *SPE Improved Oil Recovery Symposium, Tulsa, Oklahoma, USA*, 24-28 April 2010. 18, 22, 68

[40] N. Ogolo, O. Olafuyi, and M. Onyekonwu 2012, "**Enhanced Oil Recovery Using Nanoparticles**," *SPE Saudi ARabia Section Technical Symposium and Exhibition, Al-Khobar, Saudi Arabia*, 8-11 April 2012. 18

[41] S. Mokhatab, M. A. Fresky, and M. R. Islam 2006, "**Application of Nanotechnology in Oil and Gas E&P**," *JPT, Society of Petroleum Engineers*, April 2006. 18

[42] A. Maynard and E. Kuempel 2005, "**Airborne Nanostructured Particles and Occupational Health**," *Journal of Nanoparticle Science, Volume 7, Number 6*, December 2005. 18

[43] Y. D. Sun, Zheng-Ming, and H. W. Chen 2006, "**Nanotechnology Challenges: Safety of Nanomaterials and Nanomedicines**," *Asian Journal of Pharmacodynamics and Pharmacokinetics*, December 2006. 19

[44] M. L. Ostraat 2011, "**Occupational and Environmental Implications of Nanotechnology in E&P: An Overview**," *SPE Americas E&P Health, Safety, Security, and Environmental Conference, Houston, Texas, USA*, 21-23 March 2011. 19

[45] W. Zhang 2003, "**Nanoscale Iron Particles for Environmental Remediation: An Overview**," *Journal of Nanoparticle Research, Volume 5, Numbers 3-4*, August 2003. 19

[46] F. Civian 2007, "**Reservoir Formation Damage: Fundaments, Modeling, Assessment, and Mitigation**," *Elsevier Inc.*, 2007. 21

[47] C. Gao 2007, "**Factors Affecting Particle Retention In Porous Media** ," *Emirates Journal for Engineering Research, 12*, September 2007. 21, 22, 23

[48] C. Hao, E. Lange, and W. Canella 1990, "**Polymer Retention in Porous Media**," *Seventh Symposium on Enhanced Oil Recovery, Tulsa, Oklahoma, USA*, April 22-25 1990. 22

[49] S. Bolantaba, A. Skauge, and E. Mackay 2009, "**Pore Scale Modelling of Linked Polymer Solution(LPS) - A New EOR Process**," *European Symposium on Improved Recovery, Paris, France*, 27-29 April 2009. 22

[50] R. Seright and J. Liang 2009, "**A Comparison of Different Types of Blocking Agents** ," *European Formation Damage Conference, The Hauge, Netherlands*, 15-19 May 1995. 23

[51] S. Vafaei, T. B. Tasciuc, M. Z. Podowski, and A. Purkayastha 2006, "**Effect of nanoparticles on sessile droplet contact angle**," *Institute of Physic Publishing, Nanotechnology 17*, 14 April 2006. 25

[52] K. Sefiane, J. Skilling, and J. MacGillicray 2007, "**Contact line motion and dynamic wetting of nanofluid solutions**," *Advances in Colloid and Interface Science, Volume 138, Issue 2*, May 2008. 26, 69

[53] The Great Soviet Encyclopedia, "`http://encyclopedia2.thefreedictionary.com/Disjoining+Pressure`," *3rd Edition, 1970-1979*, Entered 28.04.2012. 26

[54] D. Wasan, A. Nikoloc, and K. Kondiparty 2011, "**The Wetting and Spreading of Nanofluids on Solids: Role of the Structural Disjoining Pressure**," *Current Opinion in Colloid & Interface Science*, Accepted 17. February 2011. 26, 69

[55] Berea Sandstone Petroleum Cores, "`http://www.bereasandstonecores.com/cores.php/`," Entered 15.04.2012. 27

[56] G. Aylward and T. Findlay, "**SI Chemical Data** 5th Edition," *John Wiley & Sons Australia, Ltd.*, 2002. 27

[57] American Petroleum Institute Consortium Registation 2010, "**Robust Summary of Information on Kerosene**," September 21 2010. 31

[58] O. Bakke, "**Experimental Study of Tertiary Low Salinity Waterflooding for Different Wettabilities**," *Master's Thesis*, 2009. 33

[59] Geochemical Instrumentation and Analysis, "`http://serc.carleton.edu/research_education/geochemsheets/techniques/SEM.html`," Entered 09.04.2012. 36

[60] B. Viksund, N. Morrow, S. Ma, W. Wang, and A. Graune, "**Initial Water Satuartion and Oil Recovery From Chalk and Sandstone by Sponaneous Imbibition**," *http://www.scaweb.org/assets/papers/1998_papers/SCA1998-14.pdf*, Entered 03.05.12. 54, 67, 69

[61] L. H. 2011, "**Energy Dispersice X-ray Spectroscopy (EDS) Analysis of Berea Sandstone**," 09.05.2012. 66

[62] S. Abbasi, A. Shahrabadi, and H. Golghanddashti 2011, "**Experimental Investigation of Clay Minerals' Effects on the Permeability Reduction in Water Injection Process in the Oil Fields**," *SPE European Formation Damage Conference, Noodwijk, The Netherlands*, 7-10 June 2011. 66

[63] W. Anderson 1987, "**Wettability Litterature Survey-Part 6: The Effect of Wettability on Waterflooding**," *SPE, Conoco Inc.*, 1987. 73

Appendix A

Results and Calculations

A.1 Porosity

Core	Dry weigth [g]	Lenght [mm]	Diameter [mm]	Bulk volume [cc]	Vref [cc]	Measured V [cc]	Vk [cc]	Vp [cc]	Porosity %
1	101,913	41,41	38,08	47,16	57	18,65	38,35	8,81	**18,68 %**
2	102,259	41,54	38,06	47,26	57	18,6	38,4	8,86	**18,75 %**
3	118,542	48,05	38,04	54,61	67,5	23,2	44,3	10,31	**18,88 %**
4	118,034	48,06	38,06	54,68	67,5	23,45	44,05	10,63	**19,44 %**
5	117,705	47,96	38,04	54,51	67,5	23,45	44,05	10,46	**19,18 %**
6	116,645	48,58	38,07	55,30	67,5	23,85	43,65	11,65	**21,06 %**
7	105,102	42,58	38,1	48,55	57	17,5	39,5	9,05	**18,63 %**
8	119,315	48,04	38,16	54,94	67,5	23,9	43,6	11,34	**20,64 %**
9	118,627	48,19	38,09	54,91	67,5	23,15	44,35	10,56	**19,23 %**
10	111,77	48,17	37,91	54,37	68	25,65	42,35	12,02	**22,11 %**
11	111,051	48,15	37,91	54,35	68	25,9	42,1	12,25	**22,54 %**
12	110,929	48,11	37,9	54,28	64	23,05	40,95	13,33	**24,55 %**
13	111,287	48,25	37,91	54,46	64	22,21	41,79	12,67	**23,27 %**
14	111,145	48,18	37,89	54,33	64	22,5	41,5	12,83	**23,61 %**
15	111,131	48,1	37,92	54,32	64	22,15	41,85	12,47	**22,96 %**

Table A.1: Core Data and Porosity Calculations

A.2 Air Permeability

Core	Lenght	Diameter	P1	P2	ΔP	Q	Q	k	1/Pm	Abs. Perm. ka	Liq. Perm. Kl
	[mm]	[mm]	[bar]	[bar]	[bar]	[l/min]	[cc/s]	[m^2]		[mD]	[mD]
1	41,41	38,08	1,5	1	0,5	2,95	49,17	5,16E-13	0,800	515,88	280,2
			1,7	1,2	0,5	3,22	53,67	4,85E-13	0,690	485,43	
			1,9	1,4	0,5	3,46	57,67	4,58E-13	0,606	458,38	
2	41,54	38,06	1,5	1	0,5	2,93	48,83	5,15E-13	0,800	514,53	306,34
			1,7	1,2	0,5	3,25	54,17	4,92E-13	0,690	492,01	
			1,9	1,4	0,5	3,48	58,00	4,63E-13	0,606	462,97	
3	48,05	38,04	1,5	1	0,5	2,17	36,17	4,41E-13	0,800	441,25	339,69
			1,7	1,2	0,5	2,46	41,00	4,31E-13	0,690	431,23	
			1,9	1,4	0,5	2,7	45,00	4,16E-13	0,606	415,93	
4	48,06	38,06	1,5	1	0,5	2,96	49,33	6,01E-13	0,800	601,39	327,86
			1,7	1,2	0,5	3,25	54,17	5,69E-13	0,690	569,23	
			1,9	1,4	0,5	3,47	57,83	5,34E-13	0,606	534,09	
5	47,96	38,04	1,5	1	0,5	2,57	42,83	5,22E-13	0,800	521,61	313,68
			1,7	1,2	0,5	2,84	47,33	4,97E-13	0,690	496,91	
			1,9	1,4	0,5	3,06	51,00	4,71E-13	0,606	470,50	
6	48,58	38,07	1,5	1	0,5	3,15	52,50	6,47E-13	0,800	646,57	365,1
			1,7	1,2	0,5	3,53	58,83	6,25E-13	0,690	624,63	
			1,9	1,4	0,5	3,7	61,67	5,75E-13	0,606	575,35	
7	42,58	38,1	1,5	1	0,5	2,8	46,67	5,03E-13	0,800	502,96	313,35
			1,7	1,2	0,5	3,12	52,00	4,83E-13	0,690	483,13	
			1,9	1,4	0,5	3,35	55,83	4,56E-13	0,606	455,87	
8	48,04	38,16	1,5	1	0,5	2,74	45,67	5,54E-13	0,800	553,54	343,22
			1,7	1,2	0,5	3,03	50,50	5,28E-13	0,690	527,70	
			1,9	1,4	0,5	3,28	54,67	5,02E-13	0,606	502,00	

Table A.2: Air Permeability Measurements and Calculations

Core	Lenght	Diameter	P1	P2	ΔP	Q	Q	k	1/Pm	Abs. Perm. ka	Liq. Perm. Kl
	[mm]	[mm]	[bar]	[bar]	[bar]	[l/min]	[cc/s]	[m^2]		[mD]	[mD]
9	48,19	38,09	1,5	1	0,5	2,97	49,50	6,04E-13	0,800	604,10	354,79
			1,7	1,2	0,5	3,24	54,00	5,68E-13	0,690	568,12	
			1,9	1,4	0,5	3,53	58,83	5,44E-13	0,606	543,94	
10	48,17	37,91	1,5	1	0,5	3,55	59,17	7,29E-13	0,800	728,64	367,36
			1,7	1,2	0,5	3,85	64,17	6,81E-13	0,690	681,22	
			1,9	1,4	0,5	4,12	68,67	6,41E-13	0,606	640,63	
11	48,15	37,91	1,5	1	0,5	3,57	59,50	7,32E-13	0,800	732,44	368,35
			1,7	1,2	0,5	3,83	63,83	6,77E-13	0,690	677,40	
			1,9	1,4	0,5	4,15	69,17	6,45E-13	0,606	645,03	
12	48,11	37,9	1,5	1	0,5	3,46	57,67	7,10E-13	0,800	709,66	348,45
			1,7	1,2	0,5	3,75	62,50	6,63E-13	0,690	663,05	
			1,9	1,4	0,5	4	66,67	6,22E-13	0,606	621,52	
13	48,25	37,91	1,5	1	0,5	3,4	56,67	6,99E-13	0,800	699,01	381,99
			1,7	1,2	0,5	3,72	62,00	6,59E-13	0,690	659,31	
			1,9	1,4	0,5	3,99	66,50	6,21E-13	0,606	621,45	
14	48,18	37,89	1,5	1	0,5	3,39	56,50	6,97E-13	0,800	696,68	397,03
			1,7	1,2	0,5	3,74	62,33	6,63E-13	0,690	662,59	
			1,9	1,4	0,5	4	66,67	6,23E-13	0,606	622,76	
15	48,1	37,92	1,5	1	0,5	3,41	56,83	6,99E-13	0,800	698,52	384,12
			1,7	1,2	0,5	3,76	62,67	6,64E-13	0,690	663,98	
			1,9	1,4	0,5	4	66,67	6,21E-13	0,606	620,74	

Table A.3: Air Permeability Measurements and Calculations

A.2.1 Klinkenberg Plot

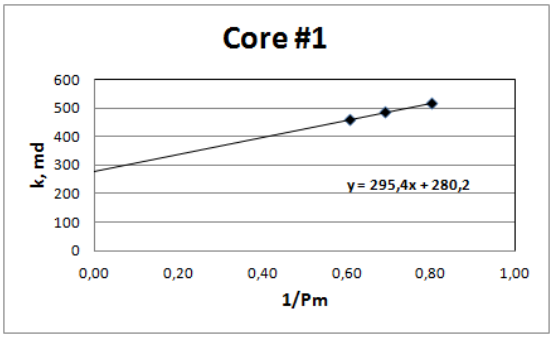

Figure A.1: Klinkenberg plot Core #1

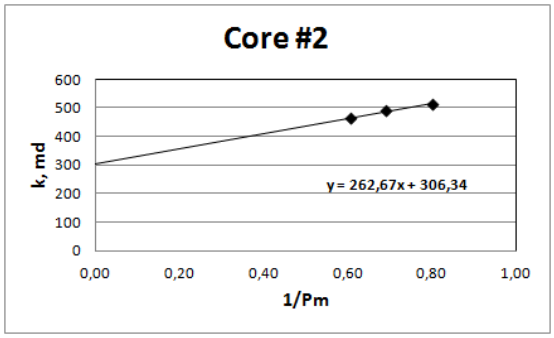

Figure A.2: Klinkenberg plot Core #2

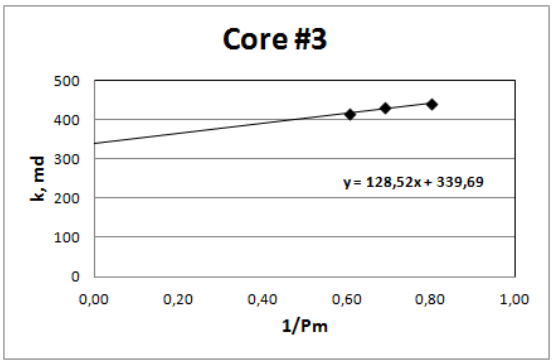

Figure A.3: Klinkenberg plot Core #3

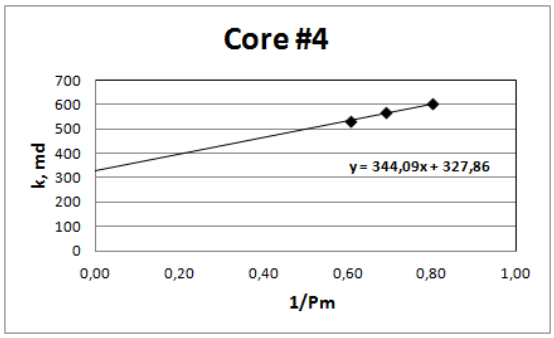

Figure A.4: Klinkenberg plot Core #4

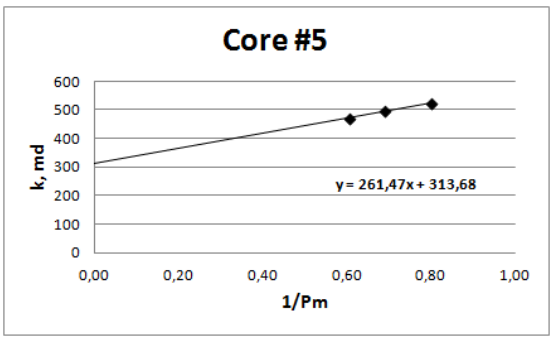

Figure A.5: Klinkenberg plot Core #5

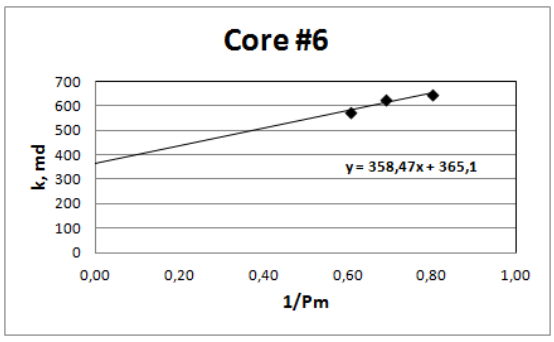

Figure A.6: Klinkenberg plot Core #6

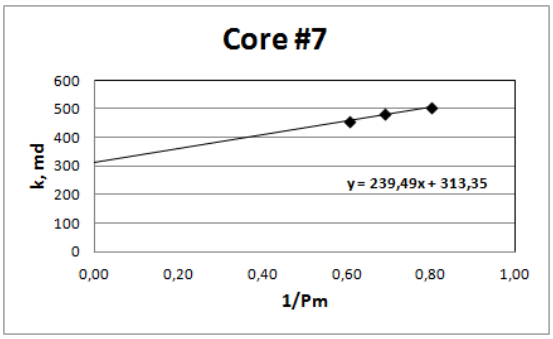

Figure A.7: Klinkenberg plot Core #7

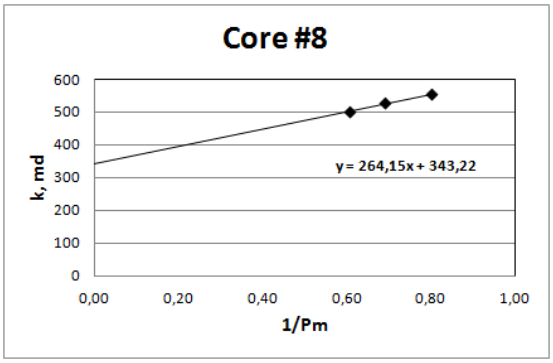

Figure A.8: Klinkenberg plot Core #8

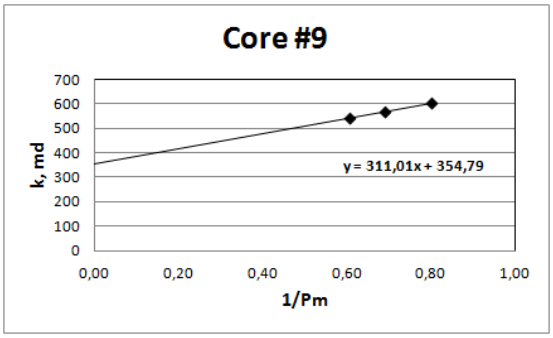

Figure A.9: Klinkenberg plot Core #9

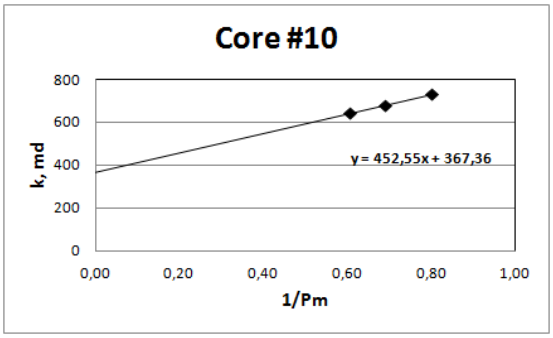

Figure A.10: Klinkenberg plot Core #10

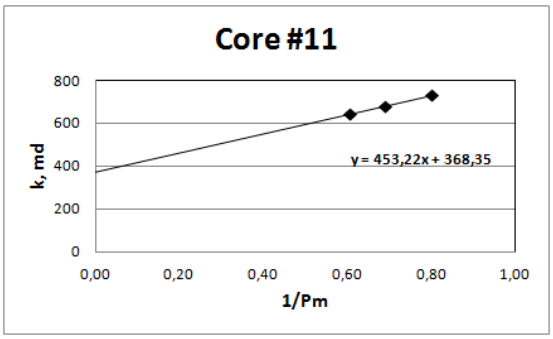

Figure A.11: Klinkenberg plot Core #11

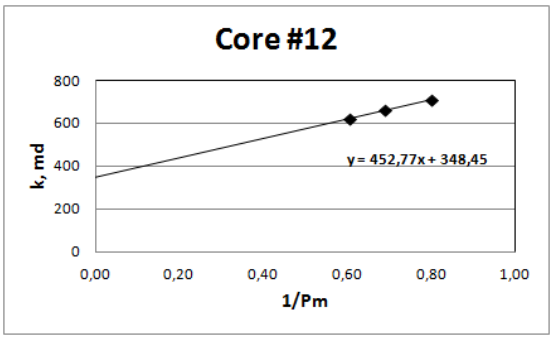

Figure A.12: Klinkenberg plot Core #12

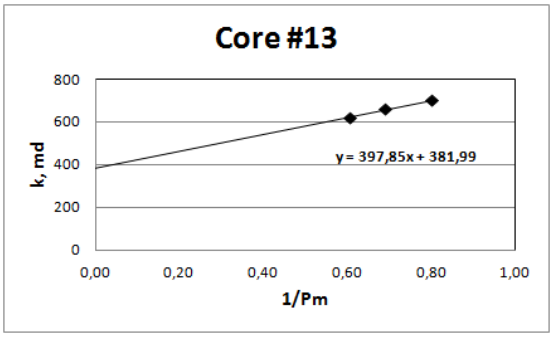

Figure A.13: Klinkenberg plot Core #13

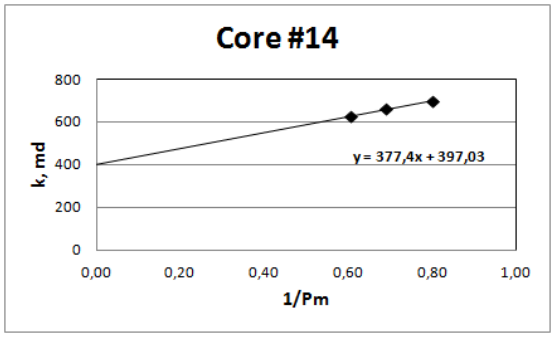

Figure A.14: Klinkenberg plot Core #14

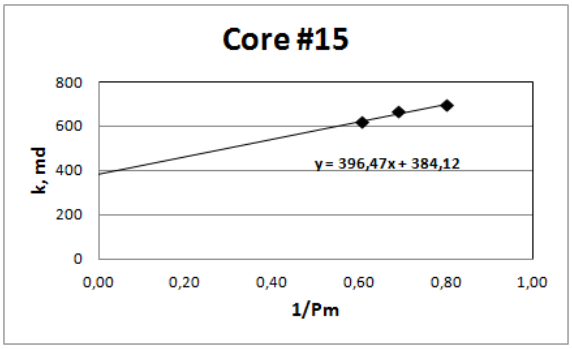

Figure A.15: Klinkenberg plot Core #15

A.3 Nanofluid

Brine Salinity	Nano concentration	Capilarry Viscometer Data				Kinematic Viscosity
wt%	wt. %	t1 [s]	k1 [mm2/s2]	t2 [s]	k2 [mm2/s2]	cSt
0,3	0,1	408	0,002452	N/A	0,001741	1,000416
	0,5	503	0,002155	640	0,001751	1,1023025
	1	572	0,002172	758	0,001707	1,268145
3	0,1	452	0,002172	598	0,001707	1,001265
	0,5	540	0,002155	735	0,001751	1,2253425
	1	702	0,002155	1058	0,001751	1,682684
10	0,1	N/A	0,002452	572	0,001876	1,073072
	0,5	532	0,002047	N/A	0,001586	1,089004
	1	635	0,002172	875	0,001707	1,4364225

Brine Salinity	Nano concentration	Weight	Nanofluid Density	Dynamic Viscosity
wt%	wt. %	g	g/cc	cp
0,3	0,1	24,662	0,998	0,998
	0,5	24,532	0,992	1,094
	1	24,561	0,994	1,260
3	0,1	25,068	1,014	1,015
	0,5	25,122	1,016	1,245
	1	25,192	1,019	1,715
10	0,1	25,401	1,028	1,103
	0,5	25,418	1,028	1,120
	1	25,481	1,031	1,481

Table A.4: Density and Viscosity Calculations for Variety of Nanofluids

Brine Salinity	Nano concentration	pH	Temperature
wt%	wt. %		C
0,3	0,1	6,02	22,1
	0,5	5,13	21,2
	1	4,71	21,1
3	0,1	5,23	21,7
	0,5	4,85	21,5
	1	4,47	21,1
10	0,1	5,36	21,1
	0,5	4,87	21,1
	1	4,42	21,1

Table A.5: pH and Temperature Readings for Variety of Nanofluids

A.4 Liquid Permeability

Core number	Length	Area	Vp	Rate water	ΔP	kabs
	[mm]	[cm2]	[cc]	[ml/min]	[mbar]	[mD]
2	41,54	11,38	8,86	0,5	10,5	**296,87**
				1	20,1	**309,37**
3	48,05	11,37	10,31	0,5	8,0	**449,21**
				1	20,0	**359,37**
4	48,06	11,38	10,63	0,5	11,5	**312,23**
				1	19,5	**368,27**
5	47,96	11,37	10,46	0,5	10,0	**358,70**
				1	23,0	**311,91**
6	48,58	11,38	11,65	0,1	4,0	**181,38**
7	42,58	11,40	9,05	0,1	5,1	**124,49**
8	48,04	11,44	11,34	0,1	3,2	**223,15**
9	48,19	11,39	10,56	0,1	3,2	**224,67**
10	48,17	11,29	12,02	0,1	8,5	**85,70**
				0,2	9,2	**157,70**
				0,5	11,3	**319,68**
11	48,15	11,29	12,25	0,1	38,9	**18,64**
				0,2	39,6	**36,65**
				0,5	38,3	**94,74**
12	48,11	11,28	13,33	0,1	12,4	**58,28**
				0,2	16,1	**90,17**
				0,5	17,2	**210,41**
13	48,25	11,29	12,67	0,1	7,8	**93,29**
				0,2	7,8	**185,70**
				0,5	10,4	**348,81**
14	48,11	11,28	12,83	0,1	41,8	**17,36**
				0,2	42,0	**34,56**
				0,5	44,3	**81,85**
15	48,1	11,29	12,47	0,1	44,8	**16,16**
				0,2	45,8	**31,65**
				0,5	47,3	**76,59**

Table A.6: Result and Calculation for Liquid Permeability Measurements

A.5 Permeability Reduction

Core number	Length	Area	Vp	Nanofluid	Rate water	ΔP	kabs	Rate Nano	Inj Nano	Rate water	ΔP Brine	kabs	K reduced
	[cm]	[cm2]	[cc]	wt%	[ml/min]	[mbar]	[mD]	[ml/min]	[ml]	[ml/min]	[mbar]	[mD]	[%]
2	41,54	11,38	8,86	0,1	0,5	10,45	296,87	0,5	26,58	0,5	236,29	13,13	**95,6 %**
					1	20,06	309,37			1	198,95	31,20	**89,9 %**
					2	35,29	351,79			2	238,07	52,15	**85,2 %**
3	48,05	11,37	10,31	0,01	0,5	8,00	449,21	0,5	5,20	0,5	51,00	70,46	**84,3 %**
					1	20,00	359,37			1	60,39	119,02	**66,9 %**
					2	40,50	354,93			2	68,99	208,35	**41,3 %**
4	48,06	11,38	10,63	0,01	0,5	11,50	312,23	0,1	5,31	0,5	15,00	239,38	**23,3 %**
					1	19,50	368,27			1	25,00	287,25	**22,0 %**
					2	31,50	455,96			2	36,00	398,96	**12,5 %**
5	47,96	11,37	10,46	0,01	0,5	10,00	358,70	0,1	2,09	0,5	20,00	179,35	**50,0 %**
					1	23,00	311,91			1	37,50	191,30	**38,7 %**
					2	45,00	318,84			2	60,00	239,13	**25,0 %**
6	48,58	11,38	11,65	0,01	0,1	4,0	181,38	0,1	2,33	0,1	4,20	172,74	**4,8 %**
7	42,58	11,40	9,05	0,01	0,1	5,1	124,49	0,1	9,05	0,1	5,8	109,47	**12,1 %**
8	48,04	11,44	11,34	0,01	0,1	3,2	223,15	0,1	2,27	0,1	3,4	210,02	**5,9 %**
9	48,19	11,39	10,56	0,05	0,1	3,2	224,67	0,1	2,11	0,1	3,8	189,20	**15,8 %**

Table A.7: Result and Calculation for Permeability Reduction Experiments with Nanofluid

A.6 Establishment of Irreducible Water Saturation

Core #10	
Rate	**Swi**
[ml/min]	**[%]**
0,5	32,61 %
1	29,28 %
2	25,12 %
4	**20,97 %**
Core #12	
Rate	**Swi**
[ml/min]	**[%]**
0,5	36,23 %
1	32,48 %
2	28,73 %
4	**26,86 %**
Core #13	
Rate	**Swi**
[ml/min]	**[%]**
0,5	32,91 %
1	28,97 %
2	25,02 %
4	**22,26 %**

Core #11 (1)			Core #11 (2)	
Rate	**Swi**		**Rate**	**Swi**
[ml/min]	**[%]**		**[ml/min]**	**[%]**
0,5	30,61 %		0,5	28,16 %
1	25,71 %		1	23,27 %
2	23,27 %		2	21,63 %
4	**20,82 %**		**4**	**18,37 %**
Core #14 (1)			Core #14 (2)	
Rate	**Swi**		**Rate**	**Swi**
[ml/min]	**[%]**		**[ml/min]**	**[%]**
0,5	22,29 %		0,5	36,87 %
1	18,39 %		1	33,75 %
2	14,50 %		2	27,51 %
4	**9,04 %**		**4**	**25,95 %**
Core #15 (1)			Core #15 (2)	
Rate	**Swi**		**Rate**	**Swi**
[ml/min]	**[%]**		**[ml/min]**	**[%]**
0,5	21,41 %		0,5	35,85 %
1	17,40 %		1	31,84 %
2	15,00 %		2	28,63 %
4	**11,79 %**		**4**	**25,42 %**

Table A.8: Results from Establishment of S_{wi} for Scenario I and Scenario II

A.7 Flooding

A.7.1 Flooding Core #10

Core #10 — **Nanofluid as tertiary recovery method**

Weight dry	111,77	[g]
Weight saturated with brine	123,145	[g]
Weight after flooding	X	[g]

Imbibition process

Time	Rate	Vo	Vw	PV	RF
[min]	[ml/min]	[ml]	[ml]		[%]
0	0,5	0	0	0	0
3	0,5	1	0	0,08	10,53 %
6	0,5	1,05	0	0,17	21,58 %
9	0,5	1,05	0	0,26	32,63 %
12	0,5	1,1	0	0,35	44,21 %
17	0,5	0,4	1,2	0,48	48,42 %
21	0,5	0,25	1,7	0,64	51,05 %
33	0,5	0,15	5,35	1,10	52,63 %
41	0,5	0	3,9	1,43	52,63 %
48	0,5	0,1	3	1,68	53,68 %
53	0,5	0	2,1	1,86	53,68 %
57	0,5	0	1,4	1,98	53,68 %
Total		5,1	18,65	1,98	53,68 %
Sor	36,61 %				

Imbibition process continued with nanofluid

Time	Rate	Vo	Vw	PV	RF
[min]	[ml/min]	[ml]	[ml]		[%]
0	0,5	0	0	1,97587354	0,53684211
5	0,5	0	1	2,06	53,68 %
10	0,5	0	1,1	2,15	53,68 %
15	0,5	0	2	2,32	53,68 %
25	0,5	0	4,7	2,71	53,68 %
29	0,5	0	2,2	2,89	53,68 %
35	0,5	0,1	3	3,15	54,74 %
45	0,5	0	4,4	3,51	54,74 %
50	0,5	0	2,4	3,71	54,74 %
60	0,5	0,05	4,3	4,08	55,26 %
65	0,5	0	5	4,49	55,26 %
71	0,5	0	2,85	4,73	55,26 %
Total		5,25	51,6	4,73	55,26 %
Sor	35,36 %				

Table A.9: Results from flooding Core #10 with brine to residual oil saturation, followed by injection of nanofluid

A.7.2 Flooding Core #11

Core #11 **Flooding with brine**

Weight dry	111,051	[g]
Weight saturated with brine	122,83	[g]
Weight after flooding	121,153	[g]

Imbibition process

Time	Rate	Vo	Vw	PV	RF
[min]	[ml/min]	[ml]	[ml]		[%]
0	0,5	0	0	0	0
3	0,5	1,25	0	0,10	12,89 %
6	0,5	1,25	0	0,20	25,77 %
9	0,5	1,3	0	0,31	39,18 %
12	0,5	1	0,2	0,41	49,48 %
14	0,5	0,25	0,4	0,46	52,06 %
18	0,5	0	1,9	0,62	52,06 %
21	0,5	0,1	1,35	0,73	53,09 %
24	0,5	0	1,45	0,85	53,09 %
30	0,5	0,05	2,95	1,10	53,61 %
39	0,5	0	4	1,42	53,61 %
48	0,5	0	4	1,75	53,61 %
57	0,5	0,1	4,1	2,09	54,64 %
Total		**5,3**	**20,35**	**2,09**	**54,64 %**
Sor	**35,92 %**				

Table A.10: Results from flooding Core #11 with brine to residual oil saturation

Core #11 **Flooding with nanofluid**

Weight dry	111,145	[g]
Weight saturated with brine	122,597	[g]
Weight after flooding	121,66	[g]

Imbibition process

Time	Rate	Vo	Vw	PV	RF
[min]	[ml/min]	[ml]	[ml]		[%]
0	0,5	0	0	0	0
3	0,5	0,9	0	0,07	9,00 %
6	0,5	0,75	0	0,13	16,50 %
10	0,5	1,5	0	0,26	31,50 %
15	0,5	1,6	0	0,39	47,50 %
18	0,5	0,2	1,3	0,51	49,50 %
23	0,5	0,4	1,9	0,70	53,50 %
27	0,5	0,15	2,2	0,89	55,00 %
31	0,5	0,2	2,1	1,08	57,00 %
40	0,5	0,15	4,15	1,43	58,50 %
48	0,5	0	4,4	1,79	58,50 %
55	0,5	0	3,4	2,07	58,50 %
Total		**5,85**	**19,45**	**2,07**	**58,50 %**
Sor	**33,88 %**				

Table A.11: Results from flooding Core #11 with nanofluid to residual oil saturation

A.7.3 Flooding Core #12

Core #12 **Nanofluid as tertiary recovery method**

Weight dry	110,93	[g]
Weight saturated with brine	122,73	[g]
Weight after flooding	120,30	[g]

Imbibition process

Time	Rate	Vo	Vw	PV	RF
[min]	[ml/min]	[ml]	[ml]		[%]
0	0,5	0	0	0	0
3	0,5	1,1	0	0,08	11,28 %
6	0,5	1,35	0	0,18	25,13 %
9	0,5	1,45	0	0,29	40,00 %
12	0,5	1,15	0	0,38	51,79 %
15	0,5	0,4	1,25	0,50	55,90 %
19	0,5	0,2	2	0,67	57,95 %
24	0,5	0,25	2,3	0,86	60,51 %
30	0,5	0,2	2,8	1,08	62,56 %
39	0,5	0,1	4,5	1,43	63,59 %
48	0,5	0,05	4,3	1,76	64,10 %
52	0,5	0,01	1,74	1,89	64,21 %
58	0,5	0	3	2,11	64,21 %
Total		**6,26**	**21,89**	**2,11**	**64,21 %**
Sor	**26,18 %**				

Imbibition process continued with nanofluid

Time	Rate	Vo	Vw	PV	RF
[min]	[ml/min]	[ml]	[ml]		[%]
0	0,5	0	0	2,11	64,21 %
5	0,5	0	1,1	2,19	64,21 %
10	0,5	0	1,55	2,31	64,21 %
20	0,5	0,05	3,9	2,61	64,72 %
30	0,5	0	3,8	2,89	64,72 %
35	0,5	0,02	3,5	3,16	64,92 %
45	0,5	0	4,6	3,50	64,92 %
55	0,5	0,02	4,1	3,81	65,13 %
62	0,5	0	4,6	4,16	65,13 %
Total		**6,35**	**49,04**	**4,16**	**65,13 %**
Sor	**25,51 %**				

Table A.12: Results from flooding Core #12 with brine to residual oil saturation, followed by injection of nanofluid

A.7.4 Flooding Core #13

Core #13 **Nanofluid as tertiary recovery method**

Weight dry	111,29	[g]
Weight saturated with brine	123,10	[g]
Weight after flooding	121,89	[g]

Imbibition process

Time	Rate	Vo	Vw	PV	RF
[min]	[ml/min]	[ml]	[ml]		[%]
0	0,5	0	0	0	0
3	0,5	1,6	0	0,13	16,24 %
6	0,5	1,6	0	0,25	32,49 %
9	0,5	1,15	0	0,34	44,16 %
13	0,5	0,75	0,9	0,47	51,78 %
18	0,5	0,2	2,05	0,65	53,81 %
22	0,5	0,15	1,6	0,79	55,33 %
28	0,5	0,15	2,2	0,97	56,85 %
39	0,5	0,15	4,7	1,36	58,38 %
50	0,5	0	4,75	1,73	58,38 %
53	0,5	0,15	1,1	1,83	59,90 %
60	0,5	0	3	2,07	59,90 %
Total		**5,9**	**20,3**	**2,07**	**59,90 %**
Sor	**31,18 %**				

Imbibition process continued with nanofluid

Time	Rate	Vo	Vw	PV	RF
[min]	[ml/min]	[ml]	[ml]		[%]
0	0,5	0	0	2,07	59,90 %
5	0,5	0	1,15	2,16	59,90 %
10	0,5	0	1,35	2,27	59,90 %
20	0,5	0	4,2	2,60	59,90 %
30	0,5	0	3,05	2,84	59,90 %
43	0,5	0	3,1	3,08	59,90 %
50	0,5	0	4,6	3,45	59,90 %
60	0,5	0	4,3	3,78	59,90 %
66	0,5	0	3,65	4,07	59,90 %
Total		**5,9**	**45,7**	**4,07**	**59,90 %**
Sor	**31,18 %**				

Table A.13: Results from flooding Core #13 with brine to residual oil saturation, followed by injection of nanofluid

A.7.5 Flooding Core #14

Core #14 **Flooding with brine**

Weight dry	111,115	[g]
Weight saturated with brine	X	[g]
Weight after flooding	X	[g]

Imbibition process

Time	Rate	Vo	Vw	PV	RF
[min]	[ml/min]	[ml]	[ml]		[%]
0	0,5	0	0	0	0
3	0,5	1,9	0	0,15	16,28 %
6	0,5	1,6	0	0,27	29,99 %
9	0,5	1,65	0	0,40	44,13 %
12	0,5	1,1	0	0,49	53,56 %
15	0,5	0,1	1,6	0,62	54,41 %
18	0,5	0,3	1,35	0,75	56,98 %
20	0,5	0,1	1,3	0,86	57,84 %
28	0,5	0,4	4,6	1,25	61,27 %
38	0,5	0,2	4,7	1,63	62,98 %
48	0,5	0	5	2,02	62,98 %
Total		**7,35**	**18,55**	**2,02**	**62,98 %**
Sor	**33,67 %**				

Table A.14: Results from flooding Core #14 with brine to residual oil saturation

Core #14 **Flooding with nanofluid**

Weight dry	111,145	[g]
Weight saturated with brine	122,91	[g]
Weight after flooding	121,578	[g]

Imbibition process

Time	Rate	Vo	Vw	PV	RF
[min]	[ml/min]	[ml]	[ml]		[%]
0	0,5	0	0	0	0
4	0,5	1,3	0	0,10	13,68 %
8	0,5	1,55	0	0,22	30,00 %
12	0,5	1,55	0	0,34	46,32 %
16	0,5	0,7	1,35	0,50	53,68 %
21	0,5	0,3	2,3	0,71	56,84 %
27	0,5	0,2	2,1	0,88	58,95 %
37	0,5	0,05	3,6	1,17	59,47 %
46	0,5	0,1	5	1,57	60,53 %
56	0,5	0,2	4,5	1,93	62,63 %
60	0,5	0	1,65	2,06	62,63 %
Total		**5,95**	**20,5**	**2,06**	**62,63 %**
Sor	**27,67 %**				

Table A.15: Results from flooding Core #14 with nanofluid to residual oil saturation

A.7.6 Flooding Core #15

Core #15 **Flooding with brine**

Weight dry	111,131	[g]
Weight saturated with brine	122,945	[g]
Weight after flooding	121,617	[g]

Imbibition process

Time	Rate	Vo	Vw	PV	RF
[min]	[ml/min]	[ml]	[ml]		[%]
0	0,5	0	0	0	0
2	0,5	0,95	0	0,08	8,64 %
4	0,5	0,6	0	0,12	14,09 %
6	0,5	0,7	0,05	0,18	20,45 %
10	0,5	1,2	0	0,28	31,36 %
13	0,5	0,8	0	0,34	38,64 %
19	0,5	0,3	1,1	0,46	41,36 %
24	0,5	0,1	2,2	0,64	42,27 %
31	0,5	0,2	4,15	0,99	44,09 %
38	0,5	0,1	3,4	1,27	45,00 %
45	0,5	0.1	2,55	1,48	45,00 %
58	0,5	0,1	5,1	1,89	45,91 %
62	0,5	0	1,8	2,04	45,91 %
Total		**5,05**	**20,35**	**2,04**	**45,91 %**
Sor	**47,71 %**				

Table A.16: Results from flooding Core #15 with brine to residual oil saturation

Core #15 **Flooding with nanofluid**

Weight dry	111,145	[g]
Weight saturated with brine	123,027	[g]
Weight after flooding	121,6	[g]

Imbibition process

Time	Rate	Vo	Vw	PV	RF
[min]	[ml/min]	[ml]	[ml]		[%]
0	0,5	0	0	0	0
4	0,5	0,7	0	0,06	7,53 %
9	0,5	1	0	0,14	18,28 %
12	0,5	1,1	0	0,14	18,28 %
15	0,5	0,95	0	0,14	18,28 %
18	0,5	0,6	0,5	0,39	46,77 %
21	0,5	0,4	0,5	0,46	51,08 %
27	0,5	0,1	2,5	0,67	52,15 %
33	0,5	0	2,8	0,89	52,15 %
42	0,5	0,1	4	1,22	53,23 %
53	0,5	0,05	4,95	1,62	53,76 %
60	0,5	0	5	2,02	53,76 %
Total		**5**	**20,25**	**2,02**	**53,76 %**
Sor	**34,48 %**				

Table A.17: Results from flooding Core #15 with nanofluid to residual oil saturation

Appendix B

Equipment Pictures

B.1 Stabilization of Nanofluids

Figure B.1: Stabilization analysis of nanofluids - Stabilization analysis of three different nanoparticles in brine prepared with 1wt% solution. From the left Elkem 999, Aerosil130 and Aerosil300.

B.2 Flooding System

Figure B.2: Permeability reduction apparatus - Picture of the equipment used for permeability reduction experiments. Keller pressure gauge connected to computer

Figure B.3: Flooding apparatus - Picture of set up of flooding apparatus. Pump connected to three out of four cylinders containing brine, oil and Aerosil300 nanofluid

B.3 SEM-apparatus

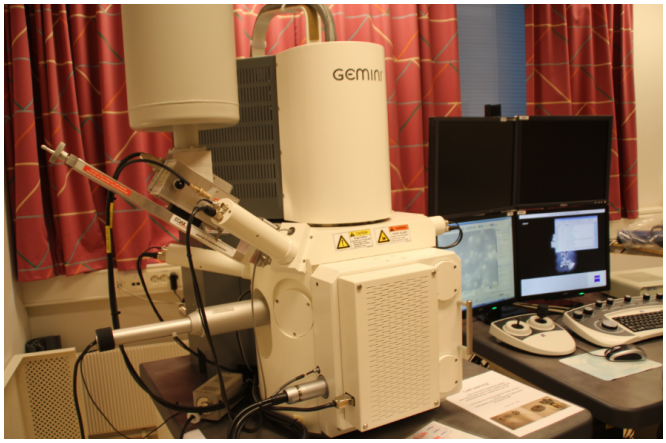

Figure B.4: SEM-apparatus - Picture of Zeiss Supra 55 VP low vacuum SEM used for analyzing of core samples after flooding

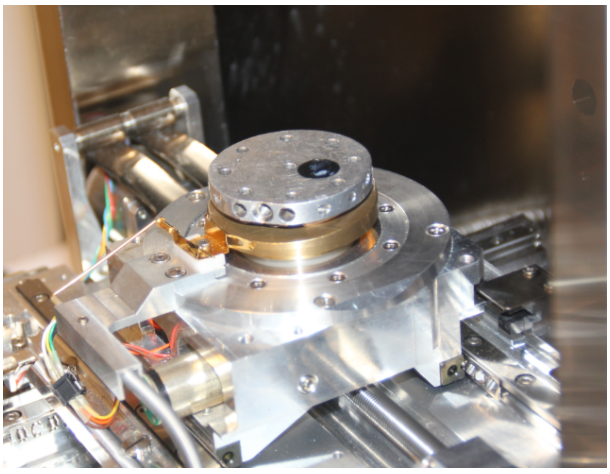

Figure B.5: Nanoparticle inside SEM - Aerosil300 nanoparticle placed on solid surface inside SEM for analyzing

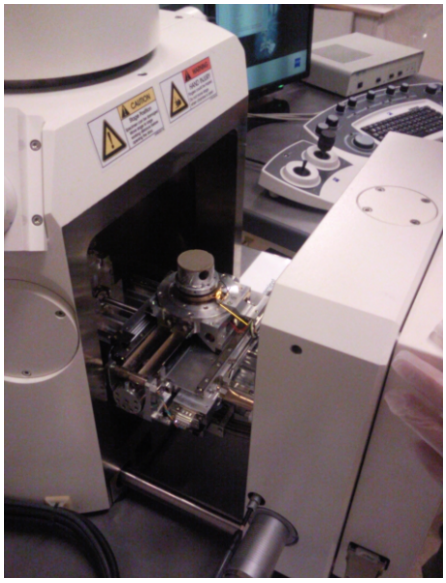

Figure B.6: Core inside SEM - A core sample placed on solid surface inside SEM for analyzing

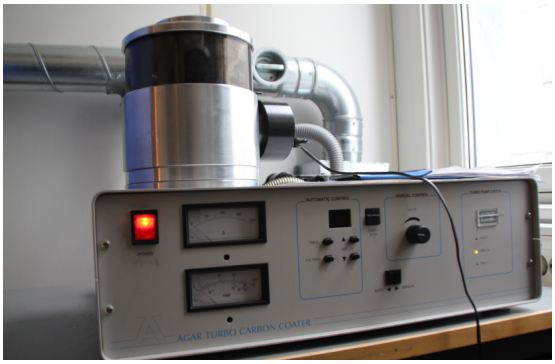

Figure B.7: Carbon-coater - Carbon-coater used for applying by a thin carbon layer onto core samples to assure conductive samples

Figure B.8: Carbon-coater - Core sample placed inside carbon-coater

Appendix C

Glossary

Al_2O_2 = Aluminium Oxide
MgO = Magnesium Oxide
Fe_2O_3 = Iron Oxide
SiO_2 = Silicon dioxide
A = Area, m^2
^{o}C = Unit of measurement for temperature
f = Flow efficency factor
^{o}K = Unit of measurement for temperature
k = Absolute permeability, m^2, mD
k_{abs} = Absolute permeability, m^2, mD
k_0 = Initial permeability
k_f = Effective permeability of a fluid
k_f = Fluid seepage
k_{rf} = Relative permeability of a fluid
L = Lenght, m
mbar = Millibar, 10^{-3} bar
μm = Micrometer, 10^{-6} m
nm = Nanometer, 10^{-9} m
ΔP = Differential Pressure, bar
P_{atm} = Atmospheric Pressure, bar
P_c = Capillary Pressure, bar
P_m = Average Pressure, bar
P_1 = Inlet Pressure, bar
P_2 = Outlet Pressure, bar
PV = Pore Volume m^3
q = Rate L/t,m^3/s
q_f = Rate of a fluid L/t,m^3/s
S_{or} = Residual oil saturation, fraction
S_g = Gas saturation, fraction
S_o = Oil saturation, fraction
S_w = Water saturation, fraction
S_{wi} = Irreducible water saturation, fraction
V_k = Reference Volume, cc
V_b = Bulk volume, cc
V_o = Volume of oil produced, cc
V_w = Volume of brine produced, cc
V_p = Pore volume, cc
V^* = Volume of particles entrapped
wt% = Weight percent

β = Surface Area Coefficient
γ = Share rate $\frac{dv_x}{d_y}$
ϕ = Porosity
ϕ_e = Effective porosity
ϕ_0 = Initial porosity
$\Sigma\Delta\phi$ = Sum of variation in porosity
μ = Viscosity, Pas, cP
μ_f = Viscosity of a fluid, Pas, cP
ρ_f = Fluid density g/cm^3
τ = Shear stress
$\sin\alpha$ = Dip anngle

Abbreviations

EOR = Enhanced Oil Recovery
ESEM = Environmental Scanning Electron Microscope
E&P = Exploration and Production
NP = Nanoparticles
PSPN = Polysilicon Nanoparticle
RF = Recovery Factor
SEM = Scanning Electron Microscopy
TEM = Transmission Electron Microscopy